UNIVERSIDAD AUTÓNOMA DE MADRID

ESCUELA POLITÉCNICA SUPERIOR

TRABAJO FIN DE MÁSTER

Hybrid experimental and model approaches for the caracterization of *Lymnaea stagnalis* neural activity

Part I: Experimental and theoretical characterisation of CPG activity in *Lymnaea stagnalis*

Máster Universitario en Investigación e Innovación en las TICs

---

Autor: Alicia Garrido Peña

Tutor: Pablo Varona Martínez
Departamento de Ingeniería Informática.

Diciembre, 2019

Abstract

Central Pattern Generators (CPG) are neural circuits that produce and coordinate rhythmic motor activity. Their robust rhythms consist of sequences of neuron activations, which result in effective motor patterns. These rhythms are at the same time flexible and can adapt as a function of the behavioral context. This work characterises the intervals that build up the rhythm and the associated sequence of the feeding CPG of the mollusc *Lymnaea Stagnalis*. The study entails both the activity obtained in electrophysiolocal recordings of living neurons and in a realistic conductance-based model. The analysis reported here assesses the quantification of the variability of the intervals and the existence of relationships between some of these intervals and the period in the form of dynamical invariants.

Keywords— CPG, Lymnaea Stagnalis, model, dynamical invariant, temporal characterisation, electrophysiology.

Resumen

Los Generadores Centrales de Patrones (CPG) son circuitos neuronales capaces de producir y coordinar actividad rítmica motora. Los ritmos robustos que presentan estos circuitos son generados por la activación secuencial de neuronas, las cuales derivan en patrones motores efectivos. Estos ritmos son capaces de adaptar la función al contexto de comportamiento gracias a su flexibilidad. En este trabajo se caracterizan los intervalos que conforman el ritmo y las correspondientes secuencias del CPG que controla la alimentación del molusco *Lymnaea Stagnalis*. Este estudio abarca tanto la actividad obtenida por medio de registros electrofisiológicos en neuronas vivas, como la obtenida a través de un modelo realista basado en conductacias. El análisis aquí presentado expone una cuantificación de la variabilidad de los intervalos, así como la existencia de relaciones lineales, en forma de invariantes dinámicos, entre algunos de los intervalos y el periodo.

Palabras clave— CPG, Lymnaea Stagnalis, modelo, invariante dinámico, caracterización temporal, electrofisiología.

Acknowledgements

First, I would like to thank this project to GNB. To Pablo, for introducing me to the Neurocomputing world, as well as all the hours spent and the trust he has put on me. Also, to Irene and Rafi, for all the hours doing experiments and for having enough patience for teaching me. To Manu and Roy for all the help with models and real-time. And, of course, to all my collegues in the lab, for receiving me this well and for making the everyday life easier.

To my family, for all the unconditional support and confidence they have always shown to me. To my parents, for listening to me and do anything they could, even in the distance, to Carmen for having always ready the exact advise and to María, for supporting me everyday and taking care of me this well.

Last, but not least, to my friends, for listening to me and worry about me anywhere they are. To the ones in the distance, for all those visits, days back home or call, that could cheer anyone up. And to you all that are here close, for all those "mind-off" moments. Specially to Maria, for all that time spent in EPS, Rodri and MAPS, for always be up to go out and have the right words. And Alvaro, for supporting and putting up with me when it is not that easy.

Agradecimientos

Me gustaría comenzar agradeciendo este trabajo al Grupo de Neurocomputación Biológica (GNB). En primer lugar, a mi tutor, Pablo, por introducirme en el mundo de la Neurocomputación, así como por todas las horas dedicadas y confianza depositada en mi. También a Irene y Rafi, por todas las horas de experimentos y la paciencia enseñándome. Y a Manu y Roy por toda la ayuda con los modelos y el tiempo real. Y, por supuesto, al resto de compañeros por acogerme tan bien en el grupo y por hacer el día a día más fácil.

A mi familia, por tanto apoyo y confianza incondicional que siempre me han dado, y que me siguen dando. A mis padres, por escucharme y hacer todo lo posible aunque fuera a la distancia, a Carmen por tener siempre el consejo adecuado y a María por aguantarme en el día a día y cuidarme tan bien.

Por último, que no menos importante, a mis amigos, por escucharme y estar pendientes de mi desde cualquier sitio. A los que están a la distancia, por esas visitas, vueltas a casa o llamadas, que reaniman a cualquiera, y a los que estáis cerca, por todos esos ratos de despeje tan necesarios. Especialmente a María, por todas horas en la EPS, a Rodri y MAPS por estar siempre dispuestos a salir y saber decirme siempre las palabras correctas. Y a Álvaro, por apoyarme y aguantarme cuando no era tan fácil.

Contents

List of Figures

1 Introduction

The project proposed for this master thesis addresses the experimental and theoretical characterisation of a central pattern generator (CPG) activity in the mollusc *Lymnaea Stagnalis*. In particular, intervals that build-up the sequence of the CPG rhythm are characterised from electrophysiological recordings and also from a realistic CPG model. The presence of dynamical invariants in the form of linear relationships between time intervals and the period is assessed. The study also includes in a second part the design of hybrid experiments to understand computational input/output relations in neural circuits.

This project is divided in two different documents to meet the requirements of the double master degree at EPS-UAM: the fist one corresponds to the present document that reports the experimental and theoretical characterisation of the intervals that build the sequence of a CPG rhythm, and the second one is entitled "Design and implementation of hybrid circuits in *Lymnaea stagnalis*" [Garrido Peña, 2019], which discusses the use of hybrid circuits built with model synapses to address the input/output response of living neurons. Both documents approach neural activity characteristics individually and in circuits from different viewpoints to assess the temporal structure of neural coding.

Here on, we will focus on the temporal characterisation of the intervals that build sequences of neural activity and the role of their interaction to build up robust motor rhythms. For this purpose, as a brief introduction to computational neuroscience, we will first review *Lymnaea* morphology and different electrophysiological recording techniques, as well as computational models to study this kind of behaviour. Then, we will characterise the sequences that underlie the CPG rhythm and discuss the presence of dynamical invariants both in the living circuit and in a CPG model.

1.1 Computational Neuroscience

1.1.1 Neural information processing

Understanding the Brain is not a new challenge in science, it has been approached in many different ways from the perspective of distinct disciplines [Kandel et al., 2012, Rabinovich et al., 2006, Dehaene, 2014]. Counting on tools from fields like biology, mathematics, physics or computer science, an interdisciplinary field as Computational Neuroscience is conformed from different sources of knowledge. It involves the assessment of neural information processing using theoretical models of neural functionality at different levels of abstraction (channels, cells, circuits, systems...) to all practical studies sustained by different measurement techniques. Furthermore, studying the brain has not only been important to get to know this organ and its functionality, but also as a basis for important progresses in several other fields. Examples of this can be found in Machine Learning with the development of Neural Networks inspired in cerebral function, which has been boosted during the last few years due to their good performance in solving complex problems. The importance of Computational Neuroscience is undeniable for all these advantages and, thanks to the fast growth of tools, technologies and computational power, this field is also growing faster everyday with important implications also in biomedical research [Fairhall and Machens, 2017].

1.1.2 Selecting data and description levels

Since the beginning of Computational Neuroscience, researches have addressed multidisciplinary subjects of study at different levels of abstraction, with their corresponding measurement and modeling techniques. The human brain is a complex system, where the activity at the cell (e.g., monitored through intra/extracellular recordings) is as important, in terms of its computational role, as the activity averaged in a whole area of the brain (e.g., as quantified in EEG or fRMI recordings). Therefore, we could classify all these different

techniques and their associated data regarding the kind of activity they measure.

Although each of the techniques used in neuroscience research are typically oriented to one specific field of study, they all have some aspects in common. What is usually measured in most of them is the voltage of the cells or a derived magnitude, which represents an overall measure of their activity. In intracellular recordings, representative informational events such as spikes or bursts are much more easy to detect and characterise [Arroyo et al., 2013, Varona et al., 2016] than events in EEG, where the recorded signal is an accumulation of the activity of up to millions of neurons [Grech et al., 2008]. Having acute recordings of spikes or bursts from one specific cell is not always required, and coarse information from one or several brain areas may be needed instead. In some cases, resolution or accuracy of some aspects of the recording might be minimised in order to obtain more informational content of a specific neural system. A similar problem is found when considering the access to the recording, or even the viability, since not all methods can be applied to the same animal models, and not all of them are easy to set up or sustain for a given experimental goal.

The issue of the different description levels not only concerns the experimental recordings, but also the use of theoretical models that formally describe different types of neuronal and neural network activity. In Computational Neuroscience literature there are two groups of model abstraction: top-down models, which describe activity, typically with a simplified approach, from general phenomena observed in some brain areas; and bottom-up models, which intend to simulate the biophysical knowledge available from ionic channels, synapses and membrane potentials. Phenomena such as neural sequence generation and coordination can be addressed both with top-down and bottom-up approaches which provide complementary views and insight [Venaille et al., 2005, Kiebel et al., 2009, Rabinovich et al., 2010, Latorre et al., 2013, Varona and Rabinovich, 2016]. In this project, bottom-up models will be used and neuronal activity from individual neurons will be accurately reproduced and their synapses and their characteristic behaviour in a circuit will also be represented in the model. Of course, bottom-up models can include insight from top-down descriptions dealing with neural dynamics, as we will also discuss below.

Theoretical models are key elements when studying brain activity. They bring in a reproduction of neural activity with full access to the dynamics of the variables that are represented in their description, and thus provide a wide variety of explorations which typically cannot be performed over *in vivo* or *in vitro* preparations. This allows a better understanding of living neural systems and their observed activity, being in many occasions a basis for a universal formalism on neural information processing. Furthermore, they are also a crucial element in hybrid circuits, where living and model neurons interact (this is widely explained in the complementary document of this project [Garrido Peña, 2019]), e.g., being able to play the role of specific neurons and synapses to realistically perturb or explore neural dynamics [Szücs et al., 2000, Amaducci et al., 2019, Reyes-Sanchez et al., 2018].

Experimental techniques might be applied in different ways, depending once again on the aim of the study. Most of them allow not only passive recording to perform offline analysis in a pure observation goal, but also interactive protocols that further contribute to characterise neural dynamics. Examples of this are close-loop and neurofeedback paradigms [Potter et al., 2014, Chamorro et al., 2012, Grosenick et al., 2015, Patel et al., 2017], where there is a dynamic interaction with the neural system under study, standing the possibility of performing online stimulation in an activity-dependent manner during the experiments. These approaches go beyond classical *in vitro* experiments and have been generalised to EEG and fMRI studies [Fernandez-Vargas et al., 2013, Karahanoğlu and Van De Ville, 2017]. These techniques have a wide range of applications, from unveiling dynamics hidden in passive recordings or traditional stimulus-response paradigms, to controlling healthy or pathological neural dynamics for a specific goal.

Here in this project, the techniques employed in the experiments and in the models will address the single cell and small-circuit description level. Intracellular and extracelullar recordings explained below will be performed in an invertebrate preparation, due to its robustness and relatively easy access. In section 1.3, we review the nervous system of *Lymnaea*, the animal model used in this study.

1.1.3 Central Pattern Generators

Central Pattern Generators (CPGs) are neural structures capable of generating rhythmic activity producing robust motor sequences in a highly autonomous manner [Hartline and Maynard, 1976, Selverston et al., 2000]. This kind of circuits is found in many different organisms, from invertebrates to vertebrates. CPGs display non-open topologies, i.e. all members of the circuit receive information from at least one other member to the circuit, which typically relies also on mutual inhibition [Huerta et al., 2001]. This characteristic endows CPGs with the ability to produce robust yet flexible rhythms where neurons negotiate the intervals that build the sequences in different behavioural contexts [Elices et al., 2019].

CPGs are believed to be the generators of rhythmical movements also in humans, e.g., in tasks such as walking, breathing, etc. Eventhough there is not as much data in humans as in animal models, there are evidences of its existence [Dimitrijevic et al., 1998] and studies that describe them a part of many neural systems [Pavlidis et al., 2016, Arichi et al., 2017] (mainly related to the locomotion function in humans). In an intuitive view, we could say that all rhythmic motor functionality that we perform unconsciously is induced by such circuits. In fact, CPGs have enough flexibility to alter their activity patterns to adapt to unexpected circumstances, e.g., to stumble while walking and restart that movement.

This is why CPGs have been taken under consideration for many years now in Neuroscience community, also in theoretical studies and robotic research [Selverston et al., 2000, Katz and Quinlan, 2019, Elices and Varona, 2015, Elices and Varona, 2017, Herrero-Carrón et al., 2011]. Even though there are obvious differences not only on the system but the functionalities between humans and different animal models, studying them on simpler individuals such as mollusc or crustacean give the chance of a deeper analysis regarding neurons interactions and intrinsic properties which generate rhythmic motor movements, and how they adapt their rhythm to alterations in their context.

When using CPGs for research, experiments are usually performed with the isolated neural system, either from physical separation in the preparation or induced by muscle relaxators. Even when isolated, CPGs still maintain their rhythm, which makes them an ideal circuit model to study neural sequence generation and coordination.

1.2 Electrophysiology

Even though electrophysiology is an area traditionally related to physiology and neurology, it is also a fundamental tool in computational neuroscience. Knowing how a system works from the associated voltage dynamics is necessary to reproduce it, as it is done with models. Additionally, advanced electrophysiological techniques are used in hybrid experiments to interact with and modify the activity of living elements [Amaducci et al., 2019]. This is why it is also important to go through the electrophysiological techniques used in this project.

Since the beginning of electrophysiology at the end of the eighteenth century, many different methods have been developed. It was Luigi Galvani who first associated some electrical phenomena involving animals nerves, observing the frog muscle contraction [Galvani, 1791]. From then on, the aim of all methods developed has been measuring these electrical flow in living circuits in order to characterise them and extract useful information about their activity [Cole, 1955, Bauer et al., 2014].

Therefore, we could say, these measures should tend to be as easy to implement as possible, trying to obtain good quality recordings to precisely characterise neural events and their temporal structure. However, when choosing these techniques, one must take into account that it is not always possible to achieve both quality and implementation ease. This is why, as it happens in many other fields, sometimes minimising quality could be an advantage if it means easier and more reproducible experiments.

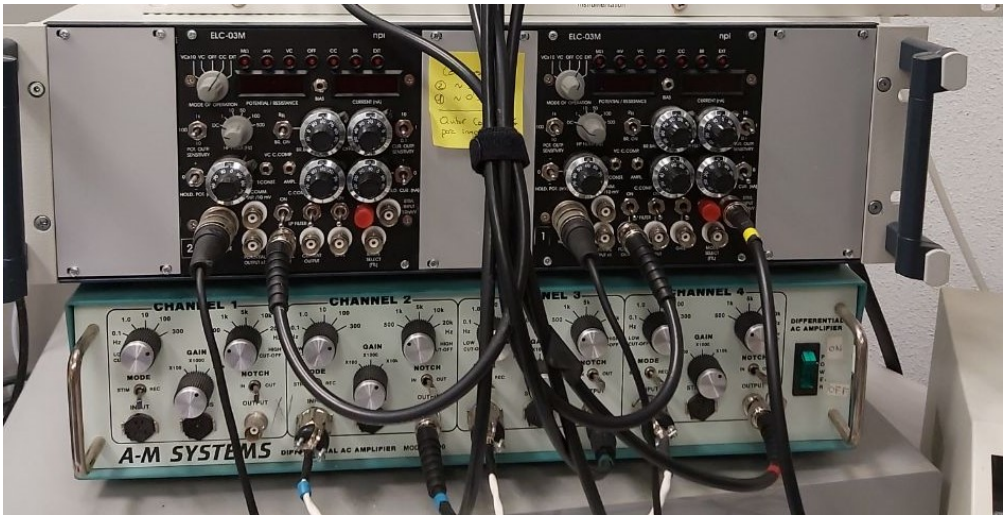

Figure 1: Intracellular (top) and extracellular (bottom) amplifiers used for the experiments reported in this project.

In overall terms, for the characterisation of the neural dynamics of the cells, specific electrodes are chosen as it is necessary to record the voltage in the biological entity. Electrodes are connected to an amplifier, which measures the potentials and injects, eventually, current modifying the neuron dynamics as we will see in next subsection. The intracelluar and extracellular amplifiers used in this study are shown in figure 1.

1.2.1 Extracellular and intracellular recording techniques

Taking into account this brief discussion on electrophysiological techniques and this duality (quality and ease), let us focus in two main groups of recordings that involve intracellular and extracellular experimental data. They both might have good performance regarding the characterisation in these experiments, and both techniques have been widely used through the years. We have knowledge on the interactions at the level of single cells and microcircuits because of these electrophysiological protocols. In figure 2 there is an example of intra- and extracelullar recordings.

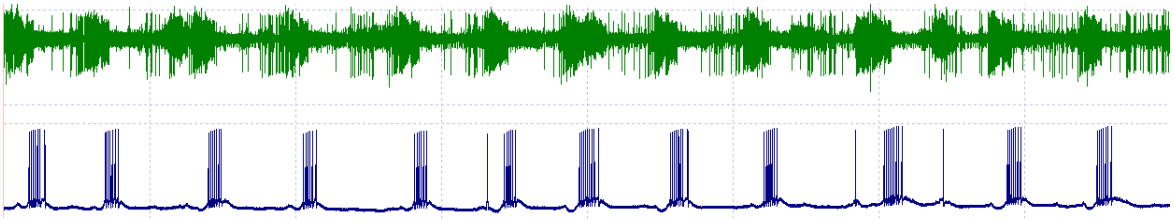

Figure 2: Example of extracellular (top panel) and intracelullar (bottom panel) neuronal electrophysiological recordings.

Extracellular recording involves all kind of techniques which use extracellular elements from the biological entity where electricity occurs, e.g. in nerves. From the data acquired by these methods, characterisations that involve spike detection can be performed. However, these recordings are usually noisy, they do not reflect the details of subthreshold dynamics, and in many cases contain the activity of several cells whose spikes have to be sorted. Therefore, when a more accurate measurement is required, e.g. one that requires

recording subthreshold neural dynamics, it is necessary to apply intracellular techniques.

Intracellular techniques, on the other hand, entail the measurement of an electrical flow in terms of current or voltage into the cell membrane. Hence, they record directly from the neuron itself, so they are much less noisy than extracellular techniques. What makes intracellular techniques interesting is not only this accurate recording, but aslso the possibility of membrane voltage control by inducing current by clamp techniques.

However intracellular recordings have also some negative aspects, as it is far more invasive than extracellular techniques, since some methods such as sharp microelectrode injection might harm the membrane. They are also more complicated to implement in the preparation, and precise manipulators are needed to impale the electrode in the neuron.

These two techniques are completely compatible, extracellular recordings might be in many occasions a perfect complement to intracellular data to study neural the system behaviour. When simultaneous recordings of several cells are required, intracellular techniques are usually not enough, since several electrodes are not always available or easy to fit in the preparation (typically no more than two to six). This is why having signals from an extracellular recording with the spike traces from one or several neurons solves this issue in many cases.

There are different techniques available to perform neuronal intracellular recordings. The technique chosen for the experiments in this project uses sharp electrodes. They were developed by Ling and Gerard in 1949 and have not had any huge change since then. The idea of these microelectrodes is to penetrate the cell membrane with its sharp tip to record the voltage minimising the damage.

For extracellular recordings, we use stainless steel electrodes isolated along with the nerve using vaselin. The application of these two techniques will be further discussed in section 2.1.

1.2.2 Clamp methods

Through the years, in the aim of studying cellular dynamics, several electrophysiological methods have been developed, leading to what we could call "modes" in measurement. These modes depend on both, the subject of study and the role of the amplifier in relation to this subject. The two classic intracellular recording modes are current- and voltage-clamp, where current and voltage are hold, respectively, and the other magnitude can be characterised [Brette and Destexhe,].

Current-clamp is well used when the only requirement is to hiperpolarize or depolarize the membrane, but not when changes in its dynamics want to be addressed. A current at a fixed value is applied to the clamped neuron, and then what changes is its voltage.

On the other hand, using voltage-clamp, current through the membrane can be measured, fixing the voltage and computing the current. Here using two electrodes (one in the case of patch-clamp), a feedback protocol can be established, receiving voltage values and adapting the current value so that the voltage value is kept over time. When having a detailed model of the conductance, this mode of measurement, contributes to the characterisation of the parameters of the model.

Based on these modes and in order to overcome the limitations of studying the dynamics of the clamped neuron individually and also in circuits, the dynamic-clamp method was invented in the early 90's [Robinson and Kawai, 1993, Sharp et al., 1993]. The set-up for this technique is pretty similar to voltage- or current-clamp, except from one important change: in this set-up current is not modulated uniquely from the amplifier but also from a computer. This allows dynamic changes and accurate simulation of artificial ionic or synaptic conductance models, and thus the implementation of hybrid circuits [Szücs et al., 2000, Amaducci et al., 2019, Reyes-Sanchez et al., 2018]. Counting on the computational power of the computer, mathematical equations of neuron models, synapses, input spikes, and complex protocols can be programmed setting

dynamically the values of the current to apply. This can be performed in an open-loop from a previously set input train or in a closed-loop activity-dependent protocol processing the voltage recorded with the computer and delivering the current to the living elements. This loop can serve to implement complex neuron and network models interacting with the living cells.

Thus, hybrid circuits relate a living entity, corresponding to the preparation of the neurons and a set-up similar to the one used in voltage- and current-clamp, and an artificial one, which is the model running on the computer, processing the input from the living neuron and computing an output according to the recorded signals in real-time. This topic is widely discussed in the complementary document of this project [Garrido Peña, 2019].

1.3 *Lymnaea* Neural System

In addition to the recording techniques' performance restrictions, there are many different issues involving the biological preparation. The fact that all these electrophysiology experiments are performed with delicate living individuals must be taking into account. This issue is, in many occasions, a huge restriction, which involves aspects regarding reproducibility and ease of the preparations and the decision on the experimental techniques that will be used. For instance, is it not the same to make recordings from mice than a crab, not only due to the distinct complexity of their neural system but for the methods used. Any research work involving animals, must follow animals treatment guidelines, where all these restrictions are contained, guaranteeing protection and welfare of animals for research purpose. In this work, we followed the guidelines from the European Commision and Universidad Autónoma de Madrid.

Figure 3: *Lymnaea Stagnalis*

Therefore, working with biological individuals with less complex neural systems has many advantages. Their welfare and manipulation involve less requirements, e.g., usually, there is no need of having a specific animal lab facilities for hosting them. Apart form that, their simple neural system is adequate when the subject of study are individual cells or their interactions in microcircuits, as in the case of CPGs. Invertebrate preparations allow studying neural dynamics from identified neurons and known connections which has had a huge impart in understanding the nervous system [Katz and Quinlan, 2019].

Due to all the advantages discussed above in addition to the ease of the associated preparation, the large size of neuron cells, the simplicity of the circuits, etc., many invertebrate spices have been studied yielding a vast amount of information regarding their morphology, electrophysiology and behaviour.

One of the invertebrate species that has been widely studied in the context of neuroscience research is *Lymnaea Stangalis*. The knowledge gathered in the last decades from this animals includes the detailed morphology of its nervous system and the the relationship of the dynamics of different circuits to several motor activities. This makes it a good candidate for the experiments addressed in this project.

1.3.1 Lymnaea morphology

Lymnaea Stangalis is a pond snail, whose neural system is shown in figure 4. As in some other molluscs, e.g. *Clione*, the neural system is conformed by several ganglia, each of them controlling (mainly, but not exclusively) some specific function of the snail. Figure 6 shows a diagram of the different ganglia which are

part of this system. The symmetry of the system can be observed in this figure. This system has two ganglia of each type, except from the visceral ganglion, all of them are interconnected by nerves. In order to have an overview of the system, bellow we will go through the different ganglia describing their main function.

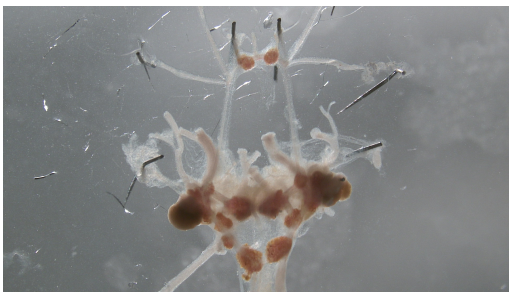

Figure 4: *Lymnaea* preparation after dissection and desheathing pinned in Petri dish.

Figure 5: Lymnaea buccal ganglia.

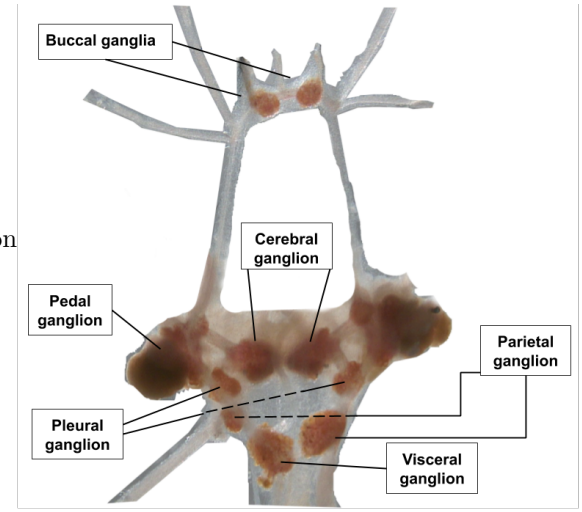

Figure 6: Lymnaea nervous system diagram.

On the upper area, we find the buccal ganglia, which control the buccal muscle involved in the processes of open-rasp-swallow, known as the feeding cycle, initiated by a CPG circuit contained in these ganglia, together with the motoneurons generating the movement, as we will discuss further on in detail. Right bellow it, two cerebral ganglia are found. They are involved in the activation and modulation of many circuits and processes. Located on the sides of the diagram, the pedal ganglia control the snail pedal movements as crawling or swimming, and they are originally joined leading to the ring shape of the system. The pleural ganglia, which contain sensory neurons, are connected to the mantle. And finally, at the bottom of the diagram, we find the parietal ganglion, involved in the control of the gill (respiratory organ) and the olfactory organ, and the visceral ganglion, connected to organs of the *Lymnaea* such as the intestine, the heart, and part of the genital apparatus.

In this work, we are going to focus in one of the ganglia containing a CPG circuit: the buccal ganglia. Our goal is to analyse and characterise the time intervals that build the sequence of its feeding cycle. This ganglia, is showed in detail in a photo taken with the microscope in figure 5. Other ganglia will be also used in the second part of this project because of the activity and shape of their neurons in relationship with the implementation of hybrid experiments [Garrido Peña, 2019].

1.3.2 Lymnaea feeding rhythm

The feeding activity of the *Lymnaea*, concerning the buccal mass, is classified in three main steps: Rest, protraction, rasp and swallow. This sequence of buccal movements in the snail is executed by the motor neurons distributed in the ganglia. Each of these phases is leaded by one interneuron from the CPG: N1,

N2, N3, and consequently, the motoneurons associated to them, which generate bursts at the same time.

In a first approach, it is easier to see this feeding as an hierarchical sequence of neuronal activations. First of all, a sensory input handled in a ganglion makes some neurons in the cerebral ganglion change their activity, consequently initiating the CPG rhythm in the N-neurons which are followed by the motoneuron rhythm. However, the activation of this circuit is not hierarchical but distributed. It has been proved that motoneurons are also implied in the feeding cycle activation [Staras et al., 1998], having some of the neurons activated simultaneously and not sequentially. Moreover, there are some neurons sucha as SO (in the buccal ganglia) or CGC (in the cerebral ganglia) which have a modulator role in the CPG, even though they are not part of it, as they have their own behaviour and function when the rhythm is inactivated.

Hence, an initial resting state, where the CPG as well as the moto-neurons have no activity, may change due to a sensory input. This input, received in the presence of food or during hunger, is handled in the cerebral ganglia generating activity and changing the SO tonic spiking during resting (which was inhibiting the CPG) to a bursting mode, meaning the start of the feeding cycle. Table 1 displays a summary of some neurons involved in each phase.

Neuron	Protraction	Rasp	Swallow
Interneuron	N1	N2	N3
	B7	B10	B3
Motoneuron	B6	B4	B9
	B1		

Table 1: Neuron participation in feeding phases.

1.4 Aim of this study

Concerning the *Lymnaea* feeding behaviour, there is a wide background knowledge on the neurons implied on the feeding cycle, which covers their individual role in the cycle, activation sequences, and morphology studies regarding their shape and configuration. Even so, there is not too much research focused on the temporal patterns of these neurons, and in particular the characterisation of the associated time intervals and their variability. In the last few years, research on this mollusc has been popular in the context of memory functions. However, temporal relations and variability of time intervals building robust sequences and the presence of universal rules of the associated information processing can also be addressed in the feeding CPG.

The groups of neurons discussed above perform all necessary functions of the snail, from eating, to crawl, or swim. In order to build such functions, the coordination of what group is activated and when is activated is crucial. The specific spatio-temporal pattern that the neurons generate is really important, as it carries key information associated to the temporal coherence of the action. This is why it is highly relevant to study the spiking bursting behaviour of the neurons, and also to address the characterisation of the sequences from the temporal structure of their constituent intervals.

Furthermore, this kind of circuits are biological networks with associated variability. Since this is an intrinsic characteristic of the behaviour, and the system works efficiently in spite of it, there might be a role for this variability in the context of the rules involved in the generation and organisation of the sequences. The study of this topic is directly related the the auto-organization of CPG dynamics as a key element of motor control.

This kind of rules has been recently discussed in the stomatogastric pyloric CPG [Elices et al., 2019]. In

particular, the presence of robust dynamical invariant intervals was shown in the pyloric CPG rhythm. The 3-phase rhythm in this system is mainly built by three neurons (LP, PY and PD). Studying cycle-by-cycle sequences, dynamical invariants in the form of linear relatioships between the LP-PD interval/delay and the period were found, while other intervals that build the sequence did not display such relation. This points out the relevance of the study of the variability of the sequence intervals and the rhythm instantaneous timing. Since these CPG generate motor movements, the sequence of neurons activation is not their only relevant feature, but also the timing of the intervals that determine when and for how long each neuron participates in each cycle of the rhythm.

In *Lymnaea* literature similar phenomena was revealed when studying the temporal feeding rhythms and its alteration applying stimulus to different neurons of the circuit [Elliott and Andrew, 1991]. Here, the feeding cycle was studied with different kinds of stimulation (stimulating N1 and SO), which induced variability, as well as in spontaneous feeding rhythms. The phase corresponding to N3 was identified as the most correlated to the period, although at that time this was not related to the concept of dynamical invariants. The aim of this project is the characterisation of the cycle-by-cycle time intervals that build the sequence of the *Lymnaea* feeding CPG and the analysis of the presence of dynamical invariants as the ones found in the pyloric CPG. This will be approached not only through experimental recordings but also in realistic *Lymnaea* feeding CPG models.

For this purpose, recordings from the *Lymnaea* buccal ganglia will be performed. Once the feeding rhythm is found, it will be characterised cycle-by.cycle from events in each neuron individually to quantify the intervals that build the sequence. We will reproduce and expand the results from Elliot et al. [Elliott and Andrew, 1991] by focusing on the variability analysis following the work of [Elices et al., 2019] in the pyloric CPG. Finally, we will perform the same analysis in a biophysical model which allows full access to all time intervals involved in the sequence.

2 Methods

This section describes the different methods used for the electrophysiological experiments done for this work with *Lymnaea* as well as the model used, along with the signal characterisation procedure applied to both.

2.1 *Lymnaea* preparation and electrophysiological recordings

As it has been mentioned before, recordings for the CPG sequence characterisation were carried out in the mollusc *Lymnaea Stagnalis* because of its easy accessible neural system, and the size and resistance of its neurons to electrode impaling.

In order to record cell signals extra- and intracellularly, it is necessary to have full access to the neurons and the nerves. This is why the central neural system (CNS), as it was shown in section 1.3, was isolated from the rest of the snail structure in all experiments reported here.

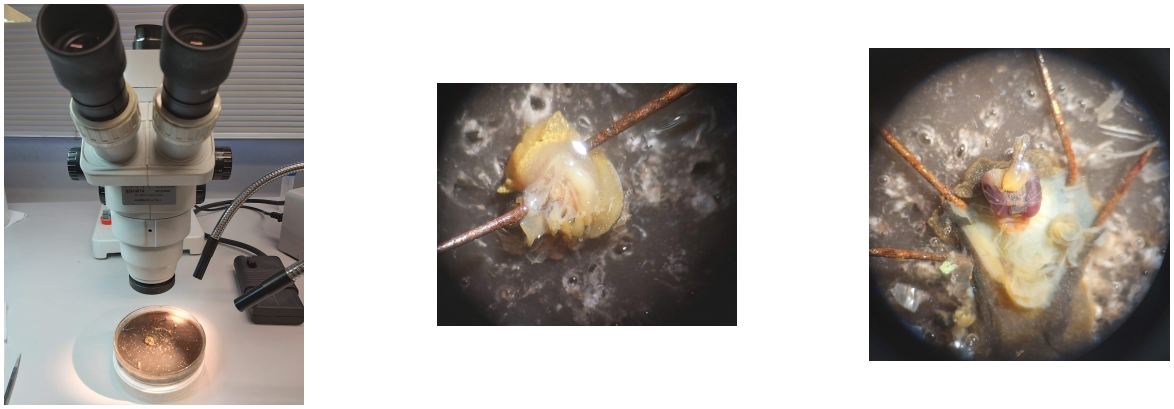

Figure 7: Dissection steps for isolating neural system. Left panel: Microscope with the preparation. Middle panel: snail after shell extraction. Right panel: buccal mass, esophagus and CNS exposed.

The first step isolating the ganglions containing the cells is extracting the snail shell and removing all unnecessary elements above the buccal system. It is important to localise the mouth and foot of the snail, since the bucall mass and CNS is right above them, so cuts must be parallel to them and as superficial as possible to avoid harming any important part of the neural system. Once the buccal mass, the esophagus and the CNS are exposed, the nerves connecting them to the rest of the pedal and buccal skin are cut. Now the only element that remains connected is the buccal mass containing all the muscles directly controlled by the buccal ganglia in the feeding cycle studied here.

Once the system is isolated by separating the nerves connected to the mass, it is important to stretch and fix the system well in the dish. This is crucial for the later manipulation and recording phases.

The intracellular technique selected in this study for recording the membrane potential of the neurons uses sharp electrodes filled with cloride solution, obtained by pulling glasses. Figures 8 and 9 show the puller machine and an example of a sharped electrode for the intracellular recordings.

As it was set out in the introduction (section 1.2), in this technique the electrodes are introduced gently into the cells, allowing the membrane potential recording while trying to minimise the harm to the cell. The *Lymnaea* ganglia are protected by a sheath above them which is thicker than in other animals used in similar electrophysiological studies. This is usually solved doing desheathing, i.e. peeling the ganglia manually removing this layer with the forceps. However, such technique is not enough for *Lymnaea* in most

Figure 8: Puller used to pull sharped micro-electrodes for the intracelluar recordings.

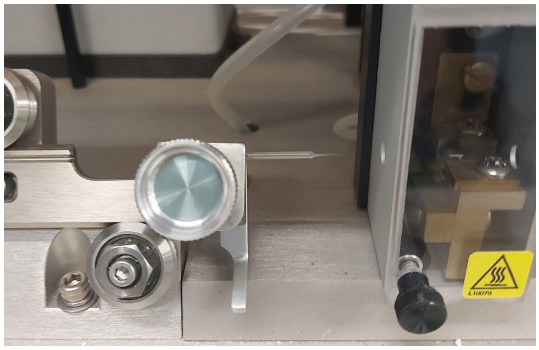

Figure 9: Example of a sharp micro-electrode.

cases and it must be complemented (or substituted) with protease application (Sigma type XIV). This is an enzyme that digests the tissue when applying a small amount on the preparation.

Besides intracellular recordings, there is also an extracellular set up which is typically used to record the activity of the nerves to identify the presence of the CPG rhythm. For its use, it is necessary to isolate the nerve to be recorded and the electrode from the rest of the preparation. This is done using vaseline surrounding both the nerve and the electrode.

For the purpose of this study, the nerves employed for the extracellular recordings are the symmetrical pair of nerves coming out from the buccal ganglia, which were originally connected to the buccal mass. Since these nerves send out the impulses to move the muscles, the neurons whose activity is recorded in the extracellular signals are mostly motoneurons [Benjamin et al., 1979], not the ones initiating the rhythm but the ones following the CPG neurons. It is important to localise these neurons in the extracellular recording for detecting the rhythm and the patterns.

Obtaining good quality recordings for the characterisation of the CPG temporal dynamics is not an easy task. On the one hand, the feeding rhythm in *Lymnaea* is pretty slow and it is not always active. In *Lymnaea* literature, several options are proposed to solve this issue. The first solution is stimulating the neurons responsible for the initiation of the feeding rhythm, such as the SO modullator neuron on the buccal ganglia or also the CBC, CVs neurons, located on brain ganglia. Stimulating these cells usually activates the target circuits [Benjamin, 2012]. However, the access to these neurons is not always easy, apart from the fact that it might be necessary to keep them in constant stimulation. Another option for activation discussed in the literature is appliying octopamine. Some neurons in the buccal ganglia are sensitive to octopamine and, as a result, this procedure activates the rhythm [Vehovszky et al., 2004]. Alternatively, some electrophysiologists leave the mouth of the snail semi-intact in order to apply sucrose resulting in the rhythm activation [Vavoulis et al., 2007, Vehovszky et al., 2004, Straub et al., 2002]. This technique, however, requires extensive experience on dissection techniques. As a foresighted option, starving the snails for three days with no food and selecting the first animal approaching the food seems to be effective for obtaining the feeding rhythm, with up to 80% of success [Elliott and Andrew, 1991].

Apart from the difficulties obtaining the rhythm, there are typically difficulties to reach the neurons. Interneurons that are part of the CPG are the smaller ones, which, concerning the electrophysiology method used in this project (sharp electrodes) increases the difficulty of the recording process. Apart from that, the motoneurons which are more directly associated to each of these interneuron feeding phase, are about the same small size, which adds to this inconvenience.

Taking all these issues and recommendations into account, recordings using the above mentioned electro-

physiological techniques can be performed. Their aim is not only recording the rhythm, but also the activity of relevant neurons that contains the right temporal reference of the feeding rhythm.

2.2 Data analysis and temporal characterisation

In a neuronal signal, there are typically two basic elements carrying the main information: spikes and bursts. A spike or action potential is a fast raise and fall in the membrane potential, typically considered as a unit of information, whereas a burst is a group of several spikes separated by a hyperpolarisation interval. CPGs typically produce spiking-bursting behaviour, which allows the recognition of well-defined time references for neural sequence analysis and characterisation [Latorre et al., 2006, Lago-Fernández et al., 2009, Elices et al., 2019].

There are several methods for detecting these events. They could be detected by a self-coded script to detect the spike peaks over a threshold. However, there are also general purpose analysis tools which include functionality for this kind of data analyses. This is the case of DataView [Heitler, 2007], defined by the authors as "a program for viewing and analyzing digital data derived from analog signals using A/D acquisition systems" [dat,]. Therefore, along with self-coded scripts, Dataview will be used for event detection in this project, due to its many possibilities on such analysis and its visualisation tools to evaluate the associated performance.

Overall, the process followed to detect the events on DataView its summed up as follows:

1. 1st derivative transformation. Derivative of the signal generates one trace containing the most significant changes of the action potential. This is important in cases such as the one shown in figure 10, where it is not possible to set a single threshold above the spikes.

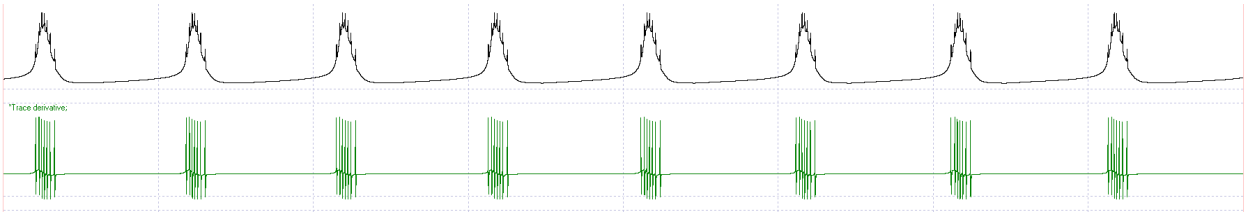

Figure 10: Spike detection from the first derivative of an intracellular recording. Black trace on the top: original signal with spikes being generated at different voltage values. Green trace: derivative of the signal where the spikes can be easily detected by a fixed threshold.

2. Threshold event detection. This tool, detects events automatically from a fixed threshold. It is ideal to detect spike events from the derivative trace. Here, it is also possible to set event duration restrictions, which might be useful in detecting bursts for non-noisy recordings. Setting the minimum time an event must be off is an easy way to differentiate from spikes and bursts. An example of spike detection using this tool is shown in figure 11.
3. Burst detection. Dataview also gives the chance to automatically detect bursts departing from the spike detection. From a channel containing the times of the spikes events, it can detect groups of them by clustering events based on some probability distribution based on the event duration selected. Options can be seen in figure 13, which displays a screenshot of the tool. This is an alternative to threshold event detection, for cases where the bursts are not that differentiated or there are remarkable frequency differences in spiking. This is the case illustrated in figure 12 where two phases are represented in the same burst, and can be detected by a change in spiking frequency.

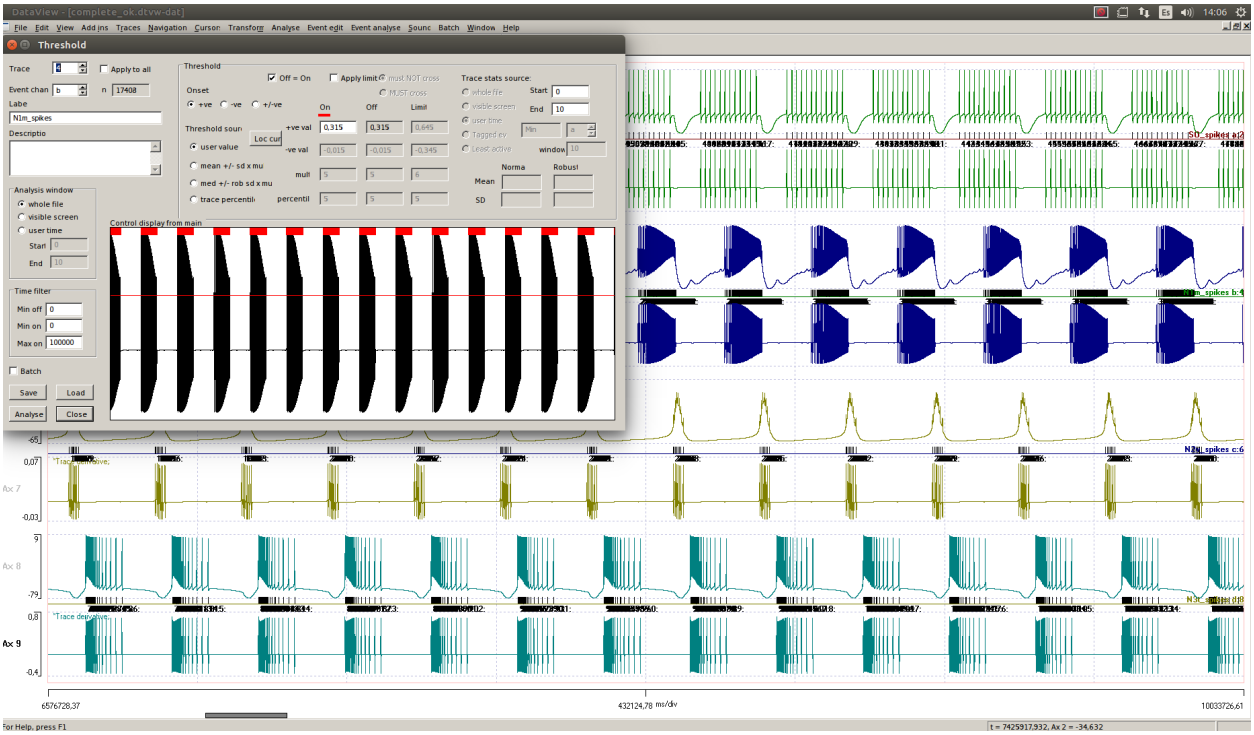

Figure 11: Dataview threshold event detection tool.

Once the events are detected, they can be exported and represented by time stamps, start time (on) and stop time. Further characterization of this data was done using Python 3.6 [pyt,]. This is a friendly language for data analysing and widely used for this purpose, and also for reading complex data files and plotting the analysis results.

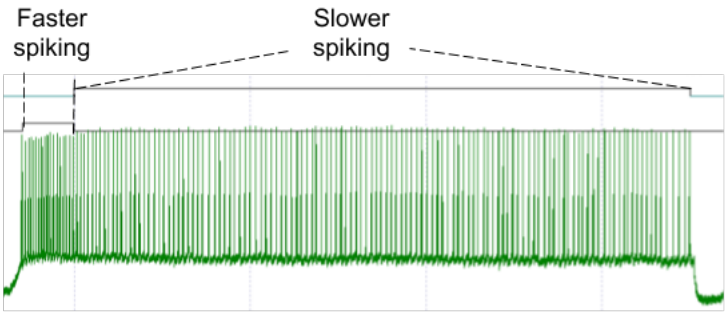

Figure 12: Example of the presence of two spiking frequencies in one same burst.

Time references, intervals and CPG sequence

As it was mentioned before in this document, this project is focused on analysing temporal intervals in the feeding CPG rhythm of *Lymnaea*, including their variability. Particularly, we assess the presence of

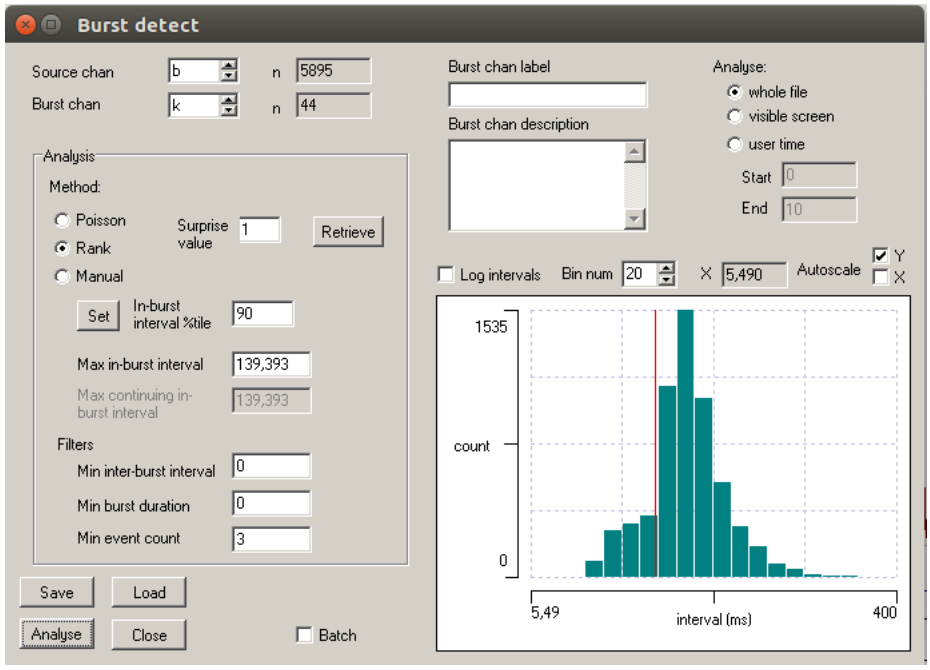

Figure 13: Dataview burst detection tool based on the spike event temporal distribution intervals.

relationships between the intervals that build the sequence and the cycle-by-cycle period to characterise and unveil similar dynamical invariants as those found in the stomatogastric CPG [Elices et al., 2019]. Hence, the burst events detected are going to be used to define three intervals in the trace of each individual neuron, and two additional intervals defined from the relation between two neurons. This is shown in figures 14 and 15, where single neuron intervals and intervals defined between neurons are represented, respectively.

Here is the definition of each interval:

1. **Burst Duration (BD)**, measured as the time interval between the first and the last spike of the burst (start to end in the trace of a given neuron).
2. **Inter burst interval (IBI)**, characterised as the difference between the last spike of a burst and the first one of the next one (end to start in the trace of a given neuron).
3. **Period**, which envelops the bursts from the three neurons, measured as the distance between the first spike of one burst in a neuron and the first spike of the next one on that neuron (start to start).
4. **NeuronX-NeuronY interval**, this interval is measured from the burst beginning of neuron X to the burst beginning of neuron Y (start X to start Y).
5. **NeuronX-NeuronY delay**, being the time lapse between the burst end of a neuron X and the burst beginning of neuron Y. (end X to start Y).

2.3 Computational model

Neural activity can be represented using mathematical models, as stated above. Thanks to their reproducibility and accurateness, they are a remarkable effective tool for studying neural behaviour.

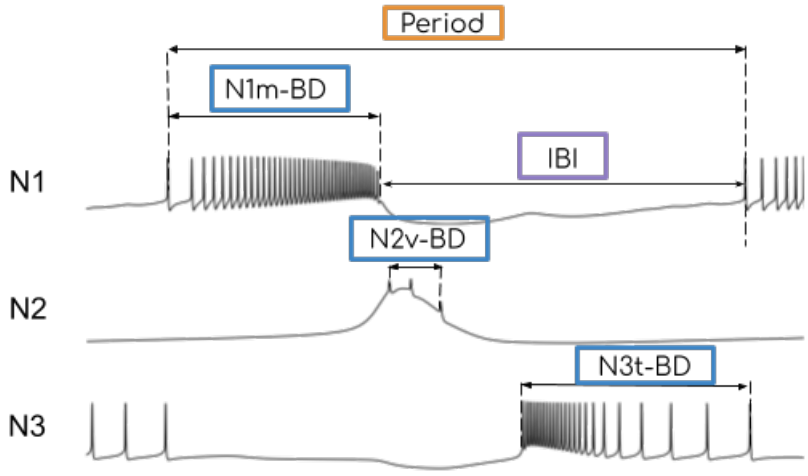

Figure 14: Individual neuron interval definition. Each BD label represents the duration of the burst, from start to end in each neuron. Period goes from N1 start to the next N1 start, covering 3 phases in relation to the activity of the other neurons. IBI represents the interburst interval, from the end to the start of the next burst in the same neuron.

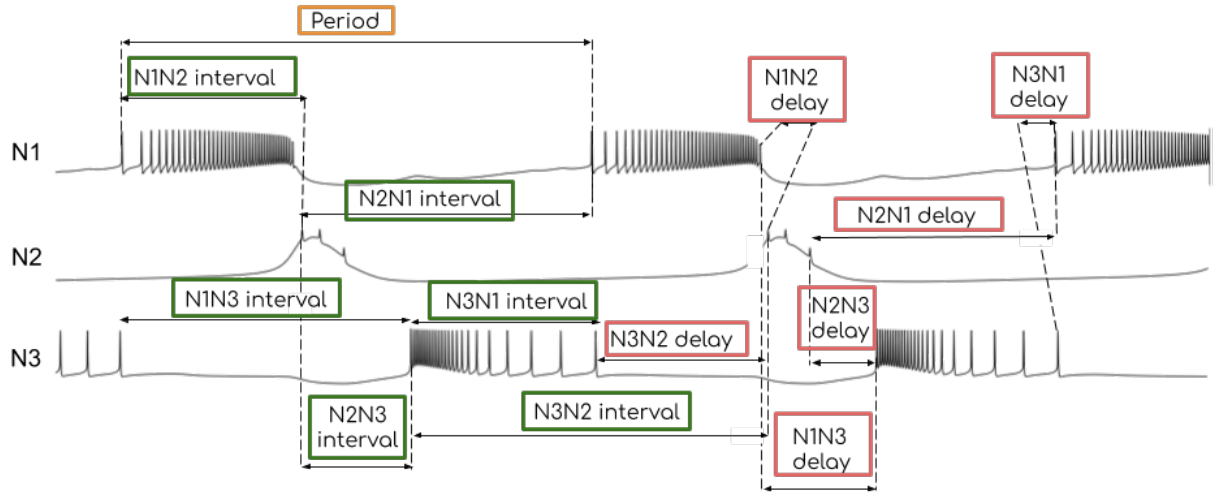

Figure 15: Definition of intervals involving pais of neurons. NXNY interval represents interval from NX start to NY start. NXNY delay represents interval from NX end to NY start. Period goes from N1 start to N1 start, covering 3 phases.

To represent the Lymnaea feeding CPG network, we will use an existing detailed model which simulates faithfully the main neurons involved in the generation of the feeding rhythm, i.e. SO, N1m, N2v and N3t (modullatory, protraction phase, rasp phase and swallow phase, respectively) [Vavoulis et al., 2007].

The model description is based on the Hodgkin-Huskley (HH) formalism [Hodgkin and Huxley, 1952] which represents single neuron biophysical properties as an equivalent electrical circuit as shown in figure 16. Adaptation of this model to specific neurons can include adding further ionic conductances besides sodium and potassium with active dependencies on the voltage or the concentration other ionic species [Torres and Varona, 2012].

In this single neuron formalism, the interaction between the voltage and the conductance variables results in the generation of neural events such as action potentials (spikes) or bursting behaviour. This interaction also shapes the temporal structure of these events as a response to a given stimulus in the form of an injected or synaptic current [Varona et al., 2001a, Varona et al., 2001b]

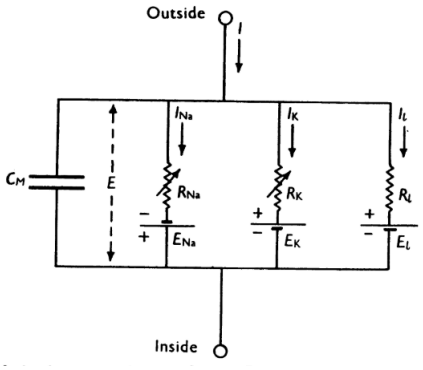

Figure 16: Hodgkin Huxley circuit [Hodgkin and Huxley, 1952]

In this work, the HH formalism is extended in a description of a snail feeding CPG by adding ionic currents representing specific behaviour for each one of the four neurons involved in the feeding rhythm. Furthermore, this model is a two compartment model which defines the soma and the axon as two differentiated structures coupled by an axial resistance, which is usually represented in models as $I_{e1} = g * (V_1 - V_2)$, where V_1 and V_2 represent the voltage in each of the two compartments and g is the coupling conductance, the inverse of the axial resistance and I_{e1} is the current that flows into one compartment from the other. This separation of soma and axon is used when it is important to differentiate between the fast and slow dynamics. In Vavoulis et al. model, this could be intuitively explained as having the slow dynamics in the soma, whereas the fast dynamics takes place in the axon compartment of the model. This distributed formalism is represented in figure 17, where each circle represents either soma or axon, with the distinct currents in each of them. The equations, corresponding to each compartment are (1) and (2) for soma and axon, respectively:

$$\tau_S \frac{dV_S}{dt} = I_{inj} - I_{L,S} - I_X - I_{ec,S} - I_{syn}, \quad with \quad I_X = [I_{ACh}, I_{NaL}, I_T] \tag{1}$$

$$\tau_S \frac{dV_A}{dt} = -I_{L,S} - I_{NaT} - I_K - I_{ec,A} \tag{2}$$

The CPG modeled here, follows the scheme shown in figure 18, where the connections between neurons are represented by dashed or solid lines, depending on whether the connection is slow or fast, and filled or empty circles at its end, denoting the direction and the effect on the postsynaptic neuron: excitation (empty circles) or inhibition (filled circles).

In addition to the distinct connections conforming the circuit, what differentiates the neuron activities in this model are the ionic channels used for modelling each of them and their corresponding parameters. The resulting difference in voltage waveform, and the effect of the connections shown in the diagram in shaping

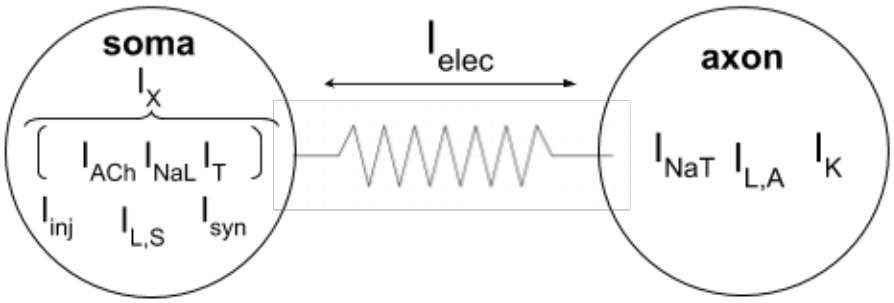

Figure 17: Ionic channel currents distribution in the two-compartment model. At the soma: I_{ACh}, acetylcholine ionic channel; I_{NaL}, slowly inactivating sodium ionic channel;I_T, low-threshold calcium current; I_{inj}, injected current; $I_{L,S}$ leakage current in soma; I_{syn} synaptic current. At the axon: I_{NaT}, fast inactivating sodium current; I_K delayed rectifier potassium current; $I_{L,A}$ leakage current in axon.

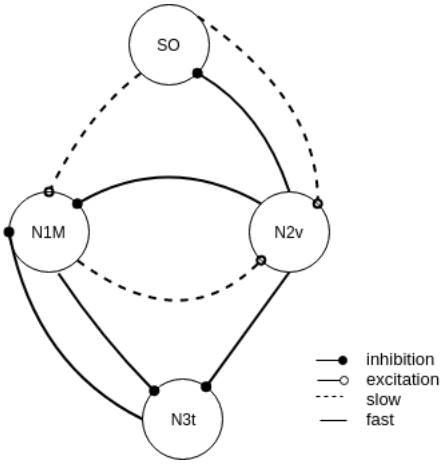

Figure 18: *Lymnaea* feeding CPG circuit.

the phase among neurons, is displayed in figure 19. The traces correspond to a simulation of the model with the complete circuit.

For a better comprehension of the model, here on, we will describe each neuron in detail, indicating the channels involved in their dynamics and their associated parameters, which shape their activity waveform and temporal structure.

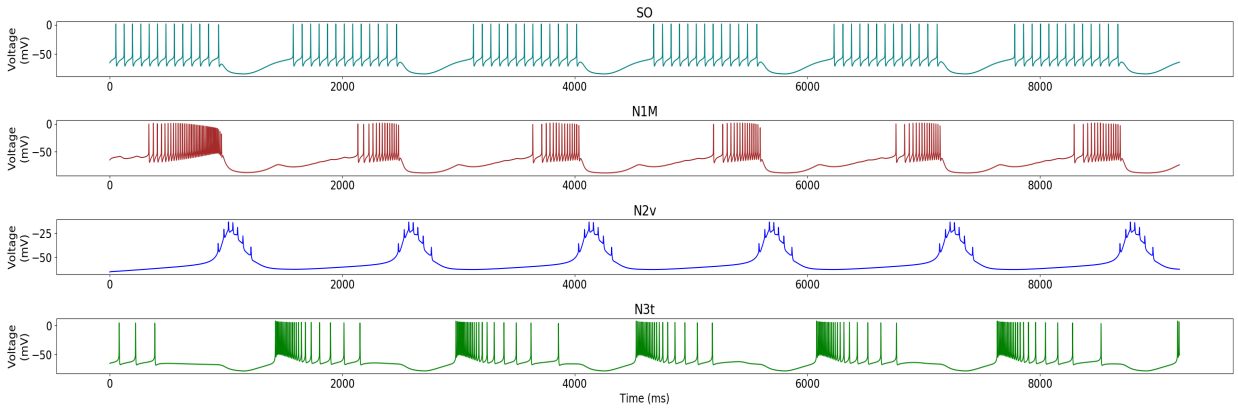

Figure 19: Complete circuit simulation example trace.

2.3.1 N1M neuron

The N1M neuron, which is in charge of the protraction phase has the particularity of a plateau, that is generated by the inhibition of the N3t neuron, as it can be seen in figure 19. The channel generating this property is I_{ACh} representing acetylcholine ion, since it is been shown it is the responsible of this plateau behaviour. The expression of this channel, as described in [Vavoulis et al., 2007] is the following:

$$I_{ACh} = 200 * p^3 * (V_s + 30) \tag{3}$$

with p a dynamic gating variable.

Therefore, N1m behaviour, has a first plateau before spiking activation, and then goes progressively increasing firing rate and decreasing in amplitude. An example of its behaviour in isolation is shown in figure 20.

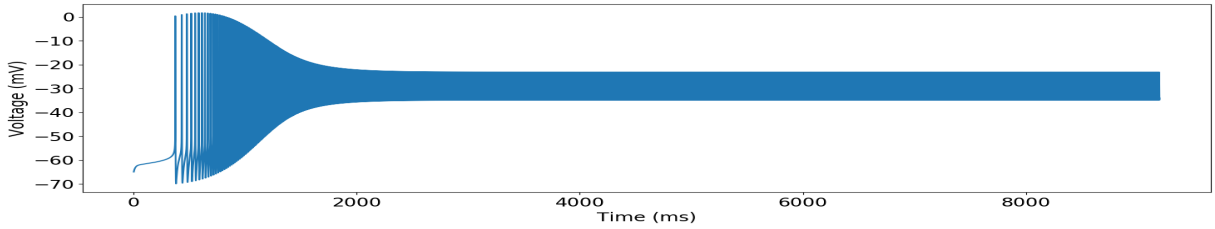

Figure 20: N1m isolated activity.

It is important to underline that thanks to that ionic current, increasing I_{inj} modifies burst duration but not this plateau effect, which will have important effects in the relation between neurons, and affecting the period. An example of this is shown in figure 21, where the I_{inj} values are 6 and 9 respectively.

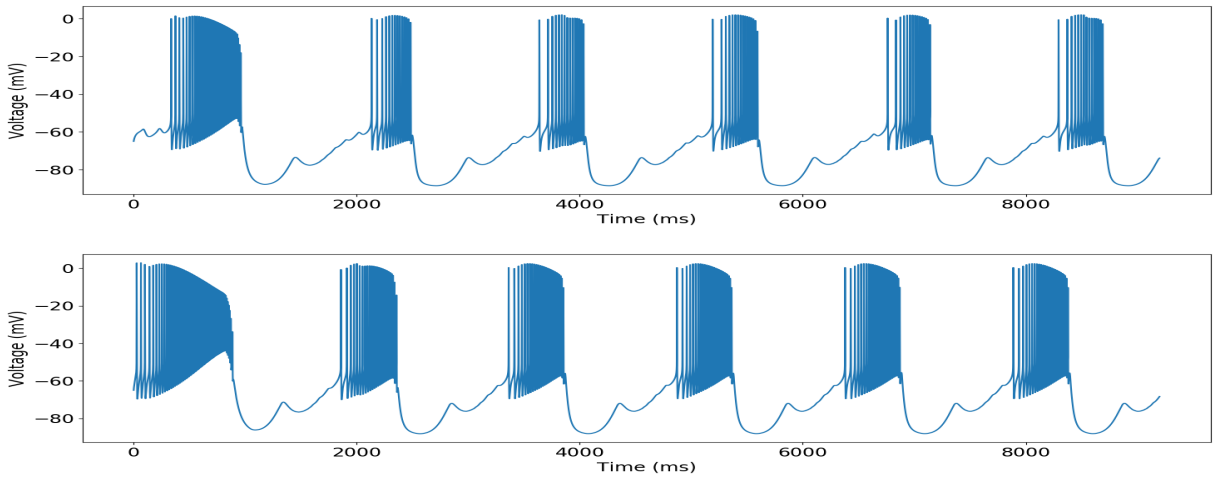

Figure 21: N1m in the complete circuit. Top: $I_{inj} = 6$; Bottom: $I_{inj} = 9$.

2.3.2 N2v neuron

N2v corresponds to the rasp phase, its characteristic trace can be seen in figure 22. As well as N1M, it has a plateau depolarisation, however, it is much shorter. The waveform in this case is more conventional, as it is exposed in [Vavoulis et al., 2007]. Its spiking activity is shorter and similar to some pyloric CPG neurons where the dynamic invariants were discovered [Elices et al., 2019].

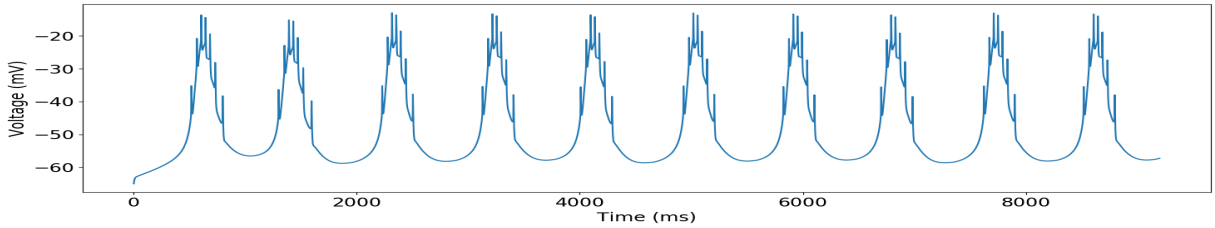

Figure 22: N2v activity.

For this purpose, an I_{NaL} (slowly inactivating sodium) current, which follows equation (4), is used to reproduce the slow activation of the neuron. Thanks to this slow activation, the spiking takes longer to start, simulating this plateau effect of the living neuron.

$$I_{NaL} = 2 * p^3 * q^3 * (V_S - 55) \tag{4}$$

On the other hand, N2v has a lower spiking frequency in the burst and thus the conductance in the electrical connection between soma and axon is lowered. In figure 23 there is an example of the effect of this conductance alteration in this neuron, changing conductance from 0.06 to 0.3, widely increasing spiking frequency, losing (consequently) some of its intrinsic properties as the plateau effect (since it starts earlier its spiking activity).

Regarding the interaction between neurons, it should be noted N2v inhibits all three other neurons involved in this circuit, being this inhibition fairly high, so it is the only neuron spiking at its time. Due to this connection, increasing the injected current ((I_{inj}) causes a higher bursting frequency in N2v and, consequently in the

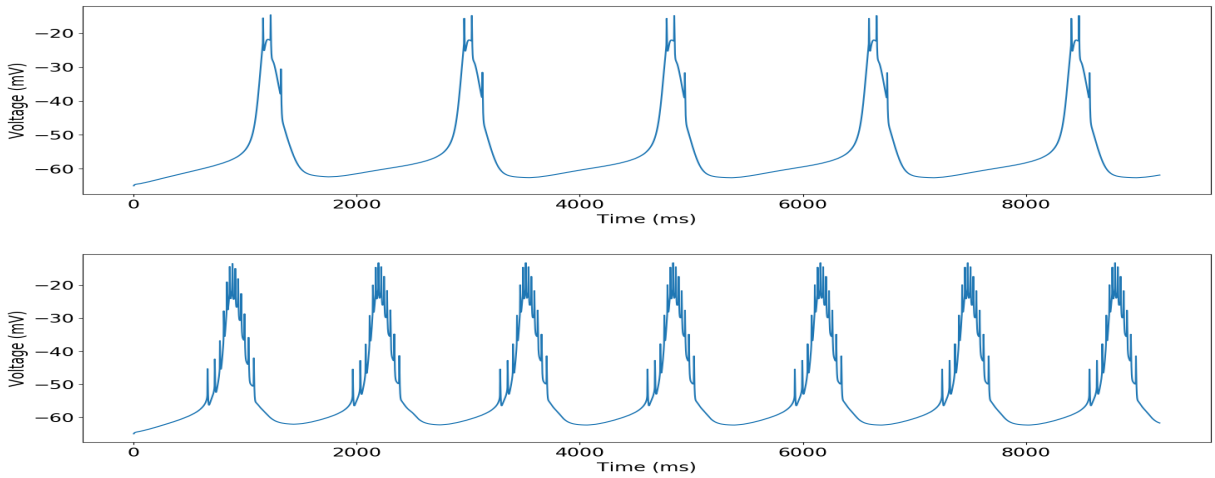

Figure 23: N2v spiking changes when the soma-axon couplling conductance is modified. Top: $g_a = 0.06$ (default); Bottom: $g_a = 0.3$.

other neurons. The bursting frequency change is shown in figure 24, where this current value changes from 2 to 4.4.

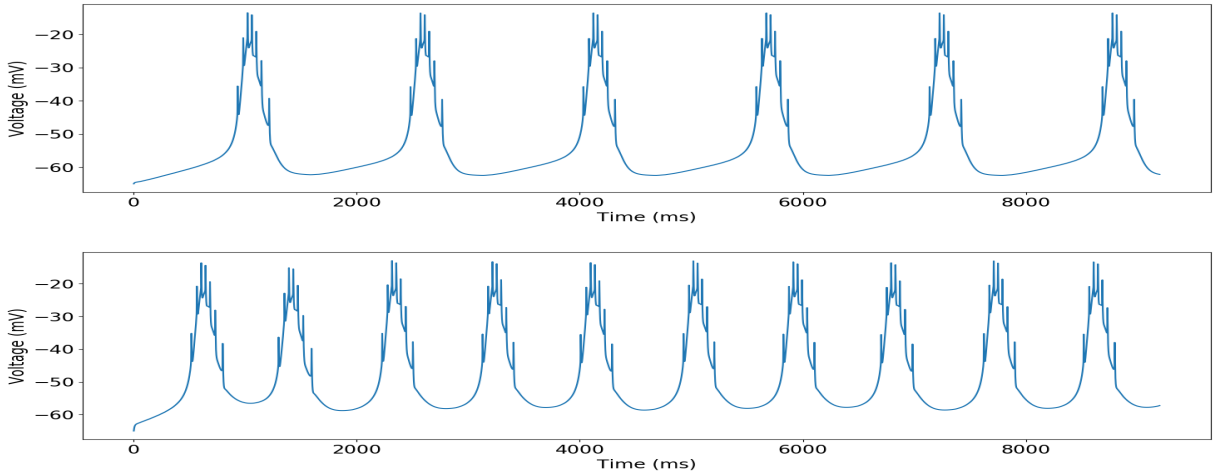

Figure 24: N2v in the complete circuit. Top: $I_{inj} = 2$; Bottom: $I_{inj} = 4.4$.

2.3.3 N3t neuron

This neuron corresponds to the last phase: swallow. In this case, what makes N3t behaviour different is a post-inhibitory rebound property, i.e. after inhibition, it experiences a high spiking frequency increase and then slows down entering a tonic spiking mode. This can be observed in figure 25.

This effect corresponds to the I_T ionic current, which is a low-threshold calcium current, as it is set out in [Vavoulis et al., 2007] with equation (5):

$$I_T = 3.27 * p^3 * q * (V_S - 80) \tag{5}$$

The relation between this current and the injected one, turns into a proportional increase of the initial higher firing frequency, as it is shown in figure 25.

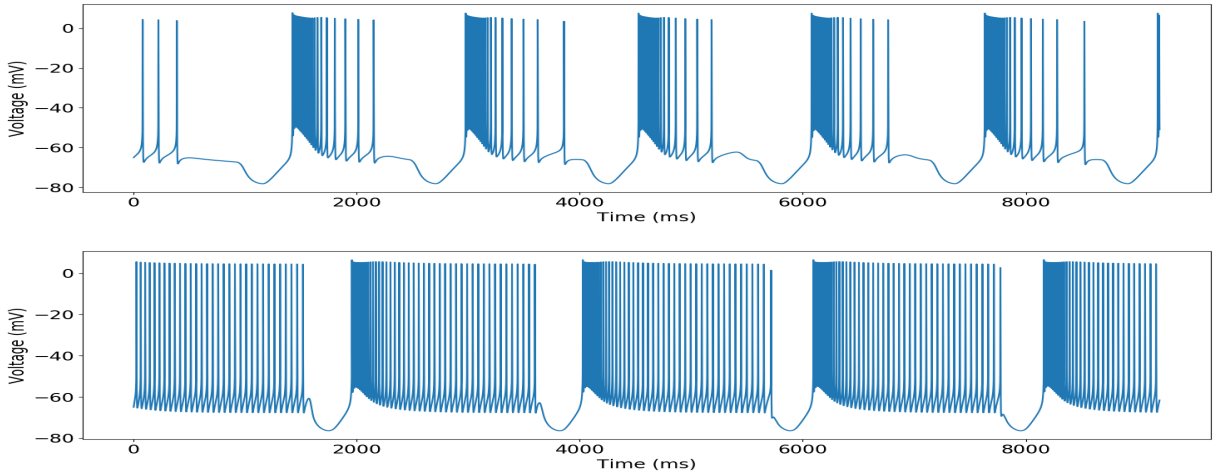

Figure 25: N3t in the complete circuit. Top: $I_{inj} = 0$; Bottom: $I_{inj} = 6$.

When interacting with the rest of the circuit, after the strong inhibition of N2v, N3t starts its activity and fires until N1M finishes its plateau and starts firing. Therefore, this neuron fits N1m plateau duration, ceasing its activity as it finishes.

2.3.4 SO neuron

Finally, the SO modulator neuron is the only one which, although being located in the buccal mass, it is not a direct part of the CPG. However, its modulatory role is important not only for controlling frequency, but also for initiating or ceseating the rhythm. When its spiking is tonic, it inhibites N1M and N2v, due to their connections shown in figure 18, and stops the feeding activity. When SO has bursting activity, its burst duration is coupled to N1M and N3t, regulating their burst duration, as it is shown in figure 26.

The SO neuron does not have any distinctive ionic current in the two compartment model. Its burst duration depends on the injected current, being shorter as I_{inj} increases. An example of its behaviour depending on this current is shown in figure 27.

The effect of this change in its burst duration is also shown in figure 26, since N1M burst duration has been reduced in order to fit both N1M and N3t in SO burst duration.

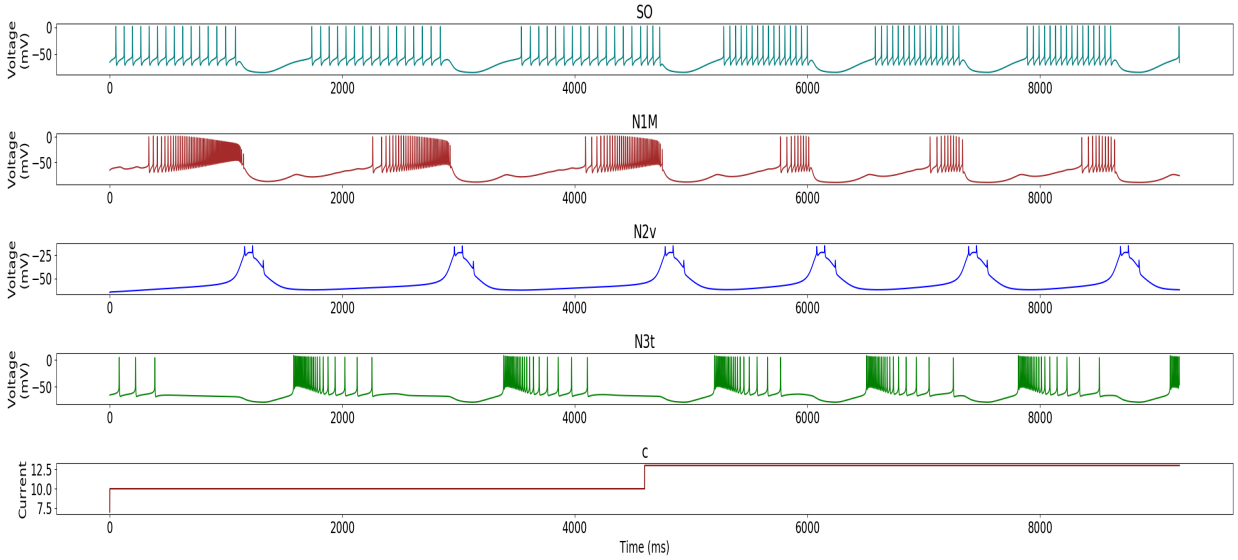

Figure 26: SO effect on the circuit, with c being the current applied to SO.

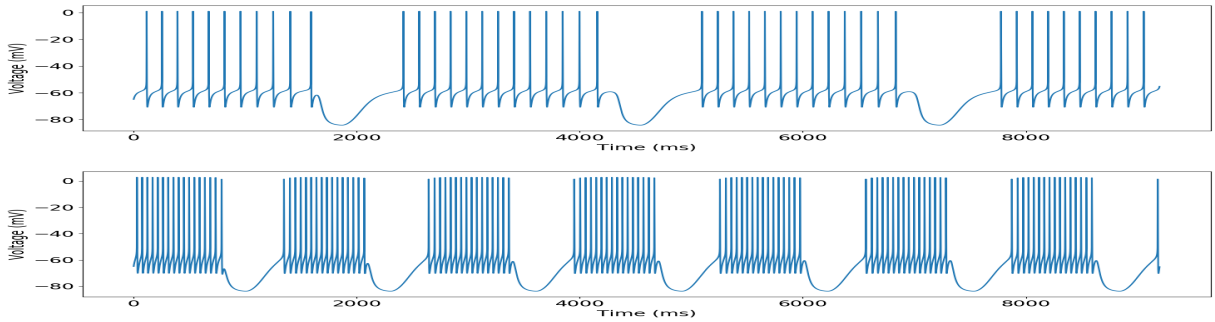

Figure 27: SO in the complete circuit. Top: $I_{inj} = 8.5$; Bottom: $I_{inj} = 13$.

2.3.5 Synapse model

The synapse used in Vavoulis et al. model is graded, in contrast to other classical synapse descriptions where the activation of the post-synaptic effect is only carried by the presence of a pre-synaptic spike [Destexhe et al., 1994]. This means that any time a spike occurs in a classical pre-synaptic neuron, the synapse current "activates" and lasts only during the pulse, since the equation representing this effect is the following:

$$dr/dt = \alpha[T] * (1 - r) - \beta * r \tag{6}$$

indicating [T] weather a pulse has occurred or not.

The main difference between this kind of synapse and the graded one used for this model is the effect of the presynaptic effect of the spike into the synapses. Instead of being 1 during the spike and 0 otherwise, the r value here, depends on the voltage value of the presynaptic neuron. In this way, not only a whole spike but also depolarization effects and low membrane potentials have a proportional effect in the post-synaptic neuron.

The equations for this type of synapes are the following:

$$\frac{dr_j}{dt} = \frac{r_{\infty,j} - r_j}{\tau_{syn,j}} \tag{7}$$

$$\frac{ds_j}{dt} = \frac{r_j - s_j}{\tau_{syn,j}} \tag{8}$$

$$r_{\infty,j} = \frac{1}{1 + e^{(-40 - V_{pre})/2.5}} \tag{9}$$

The s factor ponderates synapse current value as follows:

$$I_{syn} = \sum_j \gamma_{syn,j} s_j (V_S - E_{syn,j}) \tag{10}$$

The total I_{syn} applied to each neuron as the sum of all the synapses which affect the target neuron is shown in figure 28, where currents are displayed right bellow the neuron activity.

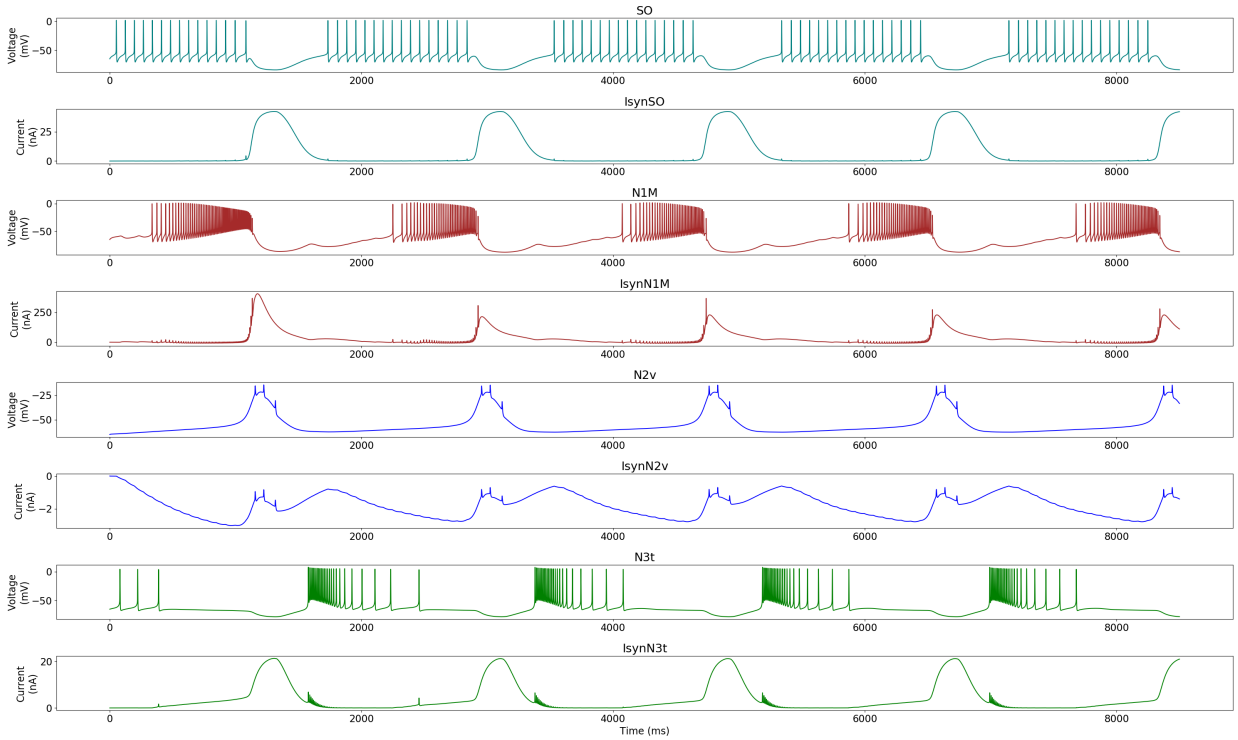

Figure 28: Complete circuit rhythm and associated currents from the input synapses.

3 Results

3.1 Sequence characterisation from intracellular recordings

3.1.1 Characterisation of time intervals building the sequence

Following the electrophysiological techniques described above, about 25 experiments were carried out with the objective of obtaining and characterising the CPG rhythm. As it has been mentioned before, obtaining this feeding rhythm is not something trivial, neither is recording two neurons simultaneously. This is why, only a few experiments provided good enough data to analyse it in terms of the interval characterisation and the assessment of the dynamical invariants. Data may not be valid for many reasons, in some experiments no phase was found, even though rhythm was present. In some other cases, where phase and rhythm were found, the recording was not long enough to obtain enough statistics, as *Lymnaea* activity was so slow that in some recordings of about 20 minutes, there where only 4 bursts. For some experiments, other technical issues appeared, such as difficulties reaching the neuron with the electrode due to a too thick sheath or soft because of the protease effect, or damage to the neural system while performing the desheathing.

The utility of the extracellular recording to check the presence of rhythm during the experiments must be emphasised. Even though the neurons present in the extracellular recording were not enough to identify the tri-phasic CPG rhythm, it was useful to discern between the presence or absence of rhythm.

One of the cases where two simultaneous intracellular recordings were in anti-phase, i.e., neurons were inhibiting each other, is shown in figure 29 with the traces plotted one over the other to visualise the details of their waveforms. In figure 30 the two recordings are superposed for a better view of their anti-phase evolution.

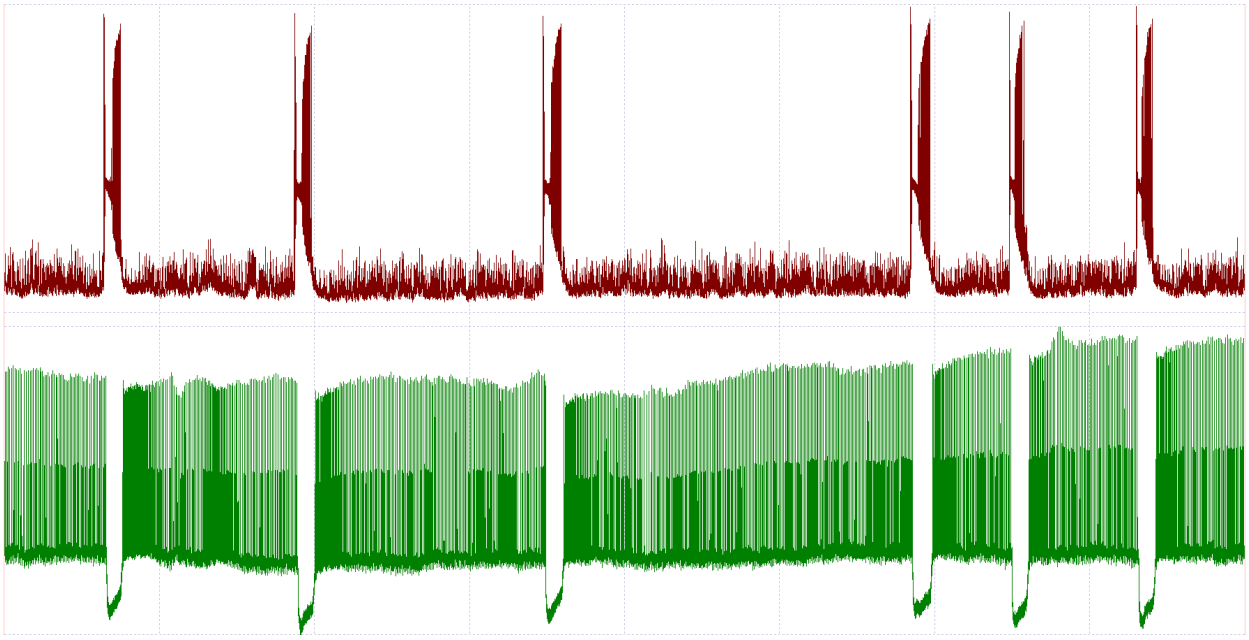

Figure 29: Representative intracelullar recordings with two neurons bursting in anti-phase.

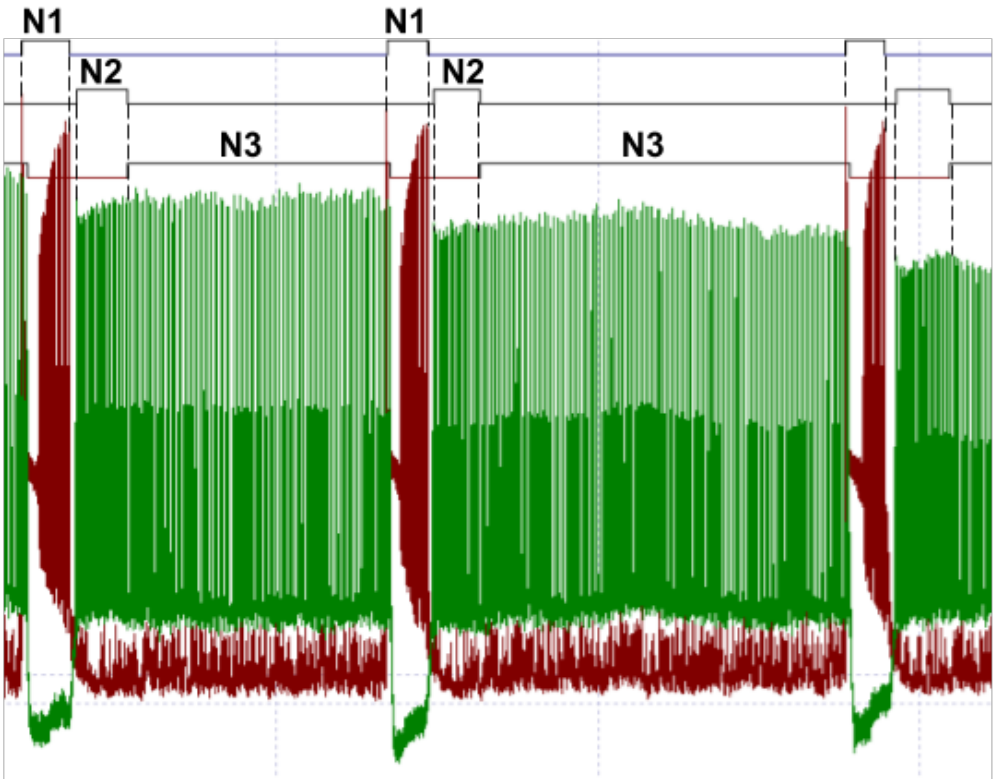

Figure 30: Three identified phases in the two intracelullar recordings with anti-phase activity.

Thus, here we have a simultaneous recordings of two neurons with antiphase activity. Although it is difficult to identify each cell with full certainty, they are supposed to be B7 and B4, both from the right buccal ganglion (N1 and N2 respectively, see table 1). As we mentioned in section 1.3, each phase of the CPG (N1, N2, N3) are followed by the respective motoneurons, which are identified by BN (B1,B3,B10...). There is a higher chance of impaling a motoneuron (due to not only their size, but also the number of neurons motoneurons available), and they can be used as a reference of each phase. We can consider them as a representation of the N cell observing the spike rate, even though they do not have the exact same duration.

By performing a frequency study in DataView for neuron 2 (green trace in figures 29 and 30), a significant change of firing rate during the burst can be observed, which might be due to the inhibition by a third neuron. Motoneurons do not necessarily have the same duration as the interneuron they follow, but they can also be active during a different interneuron burst, e.g. B4 starting along with N2 but being active (with slower activity) during N3. Therefore, here on we will assume that this recording has two separated phases, one corresponding to the fast firing and the other one to the slower phase. Thus, using this two recordings we can measure the three phases being the first one present in the the first neuron recording (red trace) and the second and the third one represented by the second neuron trace (green trace). This is illustrated in figure 30, where the three phases are labelled.

Using the techniques discussed in section 2.2 regarding the burst detection tool in DataView, it is possible to differentiate both phases in each burst, by taking their associated frequencies into account. Thanks to this distinction of two phases from a single neuron recording, it is possible to have a reference for each feeding phase of the rhythm.

Hence, having the 3-phase events detected, the variability of the distinct intervals from cycle to cycle can

be characterised, and they can be analysed comparing the correlation of each of the intervals, defined and represented in figures 14 and 15, to the instantaneous period in a cycle-by-cycle manner. Their correlation can be quantified by the R-squared value from the regression. The results for the variability analysis in this case with 32 cycles is shown in figures 31 and 32. In the first figure, a box-plot with each interval here defined displays their corresponding variability. On the one hand, the first interval shown is the period (in light orange), set as a temporal reference, this is the most variable interval, since it involves all the rest of the intervals, see figures 14 and 15.

For the other intervals, there is a remarkable difference between some of them notably variable, in contrast to other ones barely variable. The ones presenting a wider range of variability are all the intervals related with N3 bursts, which are N2-N1, N3-N1, N3-N2 intervals; N2-N1 delay and N3 burst duration. The relation of these intervals with N3 is present since they all include N3 burst duration, e.g., see N2-N1 definition in figures 14 and 15. Focusing on the N3 duration and comparing it to the analogous intervals for N1 and N2, there is a clear difference in variability, N3 has a larger difference between its minimum and maximun, as well as its data is distributed among a higher range, being its median low. The other intervals related to it have a similar distribution of the data, this can be explained because all of them integrate N3 burst duration. It is interesting to note that interval N3-N2 seems to be the most variable one, since it is covers N3 and N1, which increases its variability, being this one the closest to the period.

Regarding this variability distribution, the most variable intervals (N3-BD and related intervals) might be expected to have the strongest linear relations with the period, whereas the ones less variable (N1-BD,N2-BD and related intervals), should be the less related to the period, since their variability distribution has nothing to do with the period one.

3.1.2 Presence of dynamical invariants

Complementary to this box-plot, which represents the variability of each interval, figure 32 illustrates the correlation analysis of each cycle-by-cycle interval duration to the period. In the first row of this figure, we first see the correlation between burst duration and period, which captures a remarkably difference: N1 and N2 lack correlation with the period, and there is a strong correlation of N3 with the period. This fits with the high variability of N3 appreciated in the previous figure.

On the following rows of the panel, we find the correlation analysis of interval and delay durations against the period. Here, as we hypothesised previously, some of them also show correlation with the period, being just those involving the N3 phase. These intervals are N2-N1, N3-N1, N3-N2 intervals (third row in panel 32) and N2-N1 delay (fifth row in panel 32).

This emphasises the fact that, from the three burst duration intervals, the N3 phase seems to be the one most related to the period, as no other interval has that high correlation to the period. On the other hand, the less correlated ones are all intervals related to N1 and N2 phases, which where the ones differing the most with the period in terms of variability.

Thus, in the analysed data, the rhythm seems to have two neurons with a rather constant burst duration, whereas the third one (N3) is the most variable one, and thus most changes to the instantaneous period duration are due to this one. We can conclude this one seems to be the one carrying the period, since most of the changes in the period duration are due to this one. This is why, N3 is the most correlated with the period, obtaining a high R-squared value with its predicted regression line.

This results here exposed, are similar to the ones set out by [Elliott and Andrew, 1991], regarding the burst duration intervals, obtaining two phases not correlated with the period and the third one highly correlated. Here we have discussed these results in the context of the concept of dynamical invariants, which may underlie the functional coordination of the sequence intervals regarding which ones display a higher degree

of flexibility while keeping the robustness of the sequence [Elices et al., 2019].

The following table summarises each neuron statistics, including R-squared value and the mean and standard deviation for the three burst intervals taking into account burst duration, interburst interval (IBI) and period.

Neuron	R^2		BD	IBI	Period
N1	0.0526	**Mean**	2.6416	30.9051	33.5385
		Std	0.2884	15.0613	15.1250
N2	0.0017	**Mean**	2.9627	30.5780	33.5431
		Std	0.7409	15.1950	15.2083
N3	0.9970	**Mean**	27.2023	5.8916	33.5217
		Std	15.0324	0.7813	15.1695

Table 2: Statistics results from intracellular recording, in seconds.

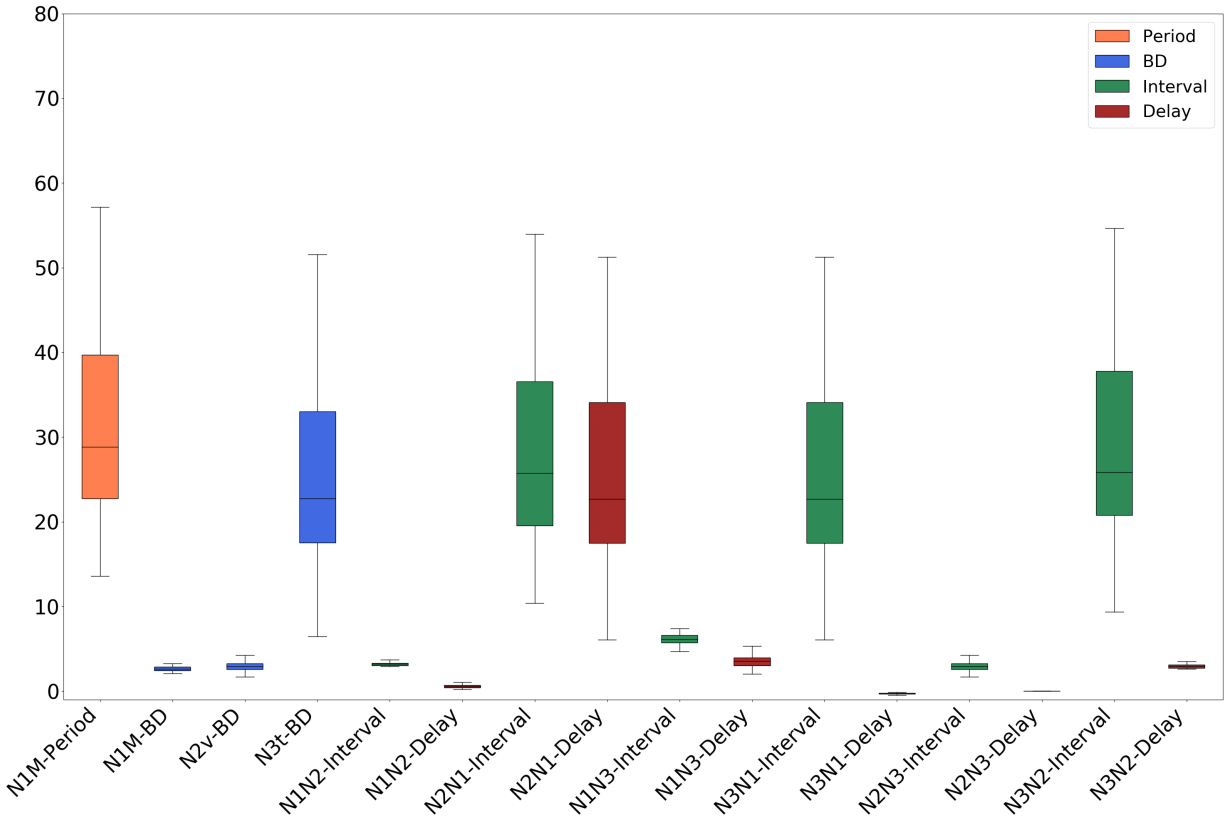

Figure 31: Box-plot representing the interval variability as measured from intracellular recordings.

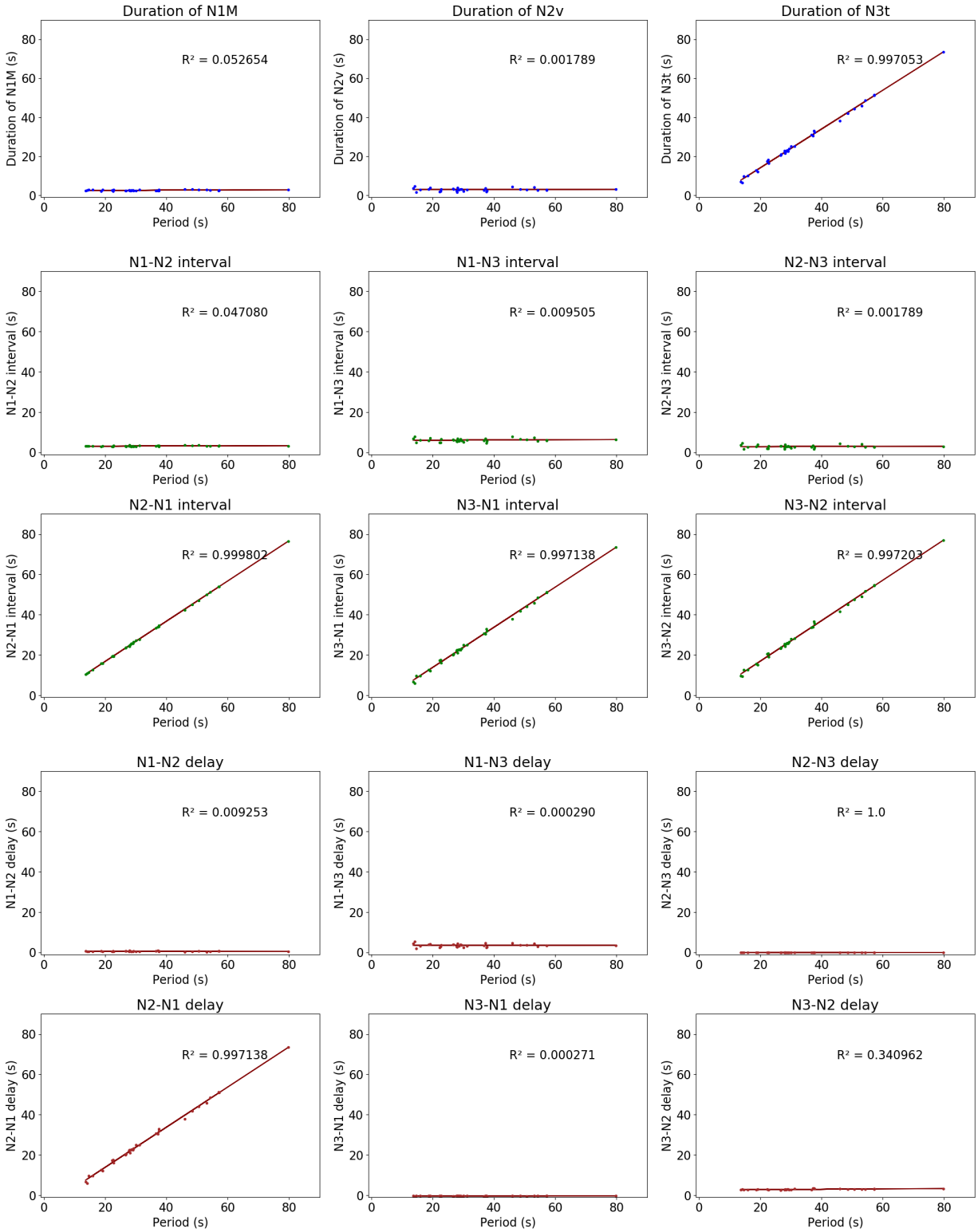

Figure 32: Intervals correlations to Period for intracellular recording. First row: Burst duration. Second and third row: Two-neuron intervals. Forth and Fifth: Two-neurons delays.

3.2 Characterisation of sequence time intervals and invariants in the computational model

From the results presented in [Elices et al., 2019, Elliott and Andrew, 1991] and in this work, it seems that the dynamical invariants are present in different biological entities. However, reproducing them in computational models is not trivial. When connecting two model neurons with an adequate network topology can result in anti-phase rhythmic behavior, However this does not mean that the duration of the associated intervals will be related to the period. Moreover, even though there are some models with intrinsic variability [Komendantov and Kononenko, 1996], it is not always possible to induce variability into a model neuron or a model circuit. As we saw in section 2.3.2, augmenting I_{inj} in the N2v neuron forces a faster bursting frequency, but it has no effect in N2v burst duration.

In the *Lymnaea* feeding CPG model [Vavoulis et al., 2007], the activity of the main neurons involved in the CPG rhythm is faithfully reproduced, including the interaction between them. Due to, not only the connections that where represented in the diagram of figure 18, but also the intrinsic activity of each neuron, the model reproduces the feeding rhythm and the correlation of some intervals with the period as described in [Elliott and Andrew, 1991].

Thanks to the current I_{inj}, variability is induced into the model, effectively changing burst duration. This current injection can be added to any model, but it does not have the same effect in all of them. Just like we saw in section 2.3, in N2v what changes is the bursting frequency, while in SO the current injection changes burst duration.

By varying the current injected into N1M, its burst duration is kept barely constant, but its plateau becomes longer. Since N3t is the neuron fitting in the sequence in that plateau, it also increases its burst duration, being the most variable one in the rhythm.

When the I_{inj} variability is over SO, it has the same behaviour that we saw in section 2.3.4. The current injection changes SO burst duration and, consequently N3t and N1M burst duration.

Here on, we are going to reproduce this effect by changing the current injection into SO and N1m. Thus, we will test the robustness of the rhythm while inducing an external perturbation that evokes variability.

Note that when the injected current has a fixed value for each neuron, the circuit does not present any variability. This is illustrated in figure 33, which displays the result of the simulation, and table 3, where some difference between intervals can be observe, but the range is so small that is irrelevant. The intervals shown in the table are the ones defined in figure 14.

Neuron	R^2		**Duration**	**IBI**	**Period**
N1	0.0070	**Mean**	0.6629	1.1519	1.8149
		Std	0.0007	0.0011	0.00001
N2	0.0003	**Mean**	0.1647	1.6500	1.8148
		Std	0.00003	0.00007	0.00003
N3	0.0132	**Mean**	0.7105	1.1042	1.8148
		Std	0.0013	0.0013	0.00001

Table 3: Statistics results from fixed current injection applied to each neuron, in seconds.

Therefore, to induce variability in the model, a variable c which controls the current injection amplitude is increased from a minimum to a maximum value, and then decreased back to the initial value. The value is increased each N3t burst (aprox.). The minimum and maximum values vary and have been chosen experimentally depending on the effect of the injected current on the neuron and ensuring burst generation

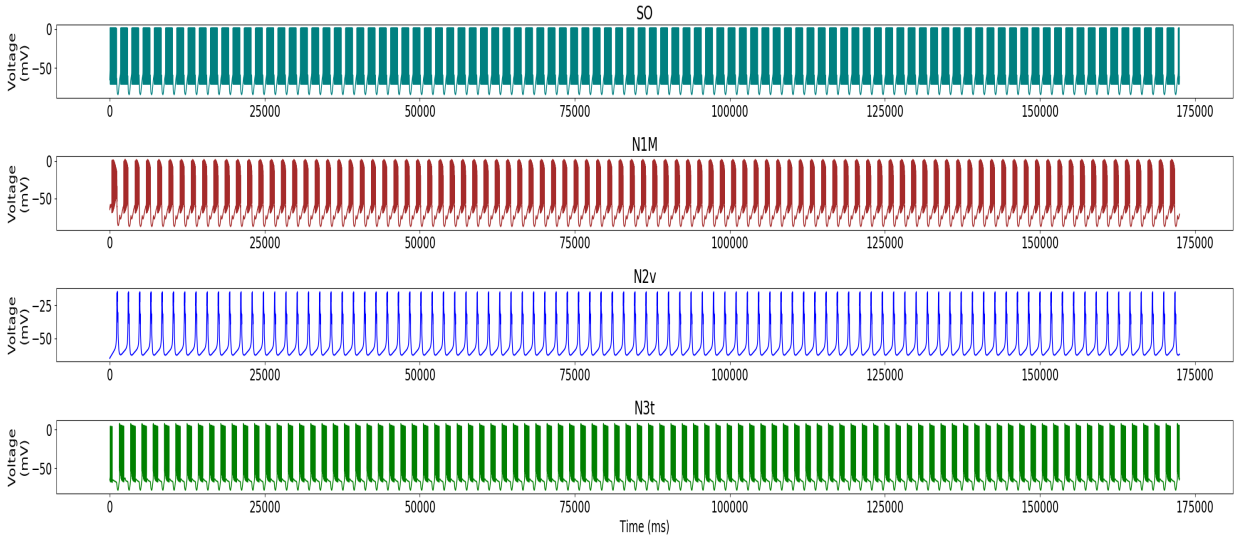

Figure 33: Complete circuit rhythm obtained by applying a **fixed** current value to each neuron.

in all neurons.

3.2.1 N1m driven activity

Setting the variable c into the N1M neuron, as the I_{inj} current, produces the result shown in figure 34, where the last row displays the current c applied.

Using the same procedures as with the recordings from the living neuron, spike and burst events have been detected for each neuron. From this data, all intervals represented in figures 15 and 14 have been quantified. Using the self-programmed script, the variability and the correlation between the period and each interval has been computed, leading to the result shown in figures 35 and 36.

In the box-plot, similar results to the intracellular recording analyses (see 3.1) can be observed (regarding variability, not intervals duration). From the three burst duration intervals, the most variable one is the one corresponding to N3t neuron, since this is the one showing a wider range of values, presenting a larger difference between its maximum and minimum. Furthermore, the derived intervals which cover N3 burst duration are also the ones presenting more variability, which also corresponds to what was found in the *in vitro* recording. However, the model data seem to be concentrated closest to the minimum. The distribution found in intervals N2-N1, N3-N1, N3-N2 intervals and N2-N1 delay, is equivalent to the one in period interval, being once again, the N3-N2 interval the more similar one. Hence, the linear relations are more likely to appear in these intervals whose distribution is closer to the period.

On the other hand, the less variable intervals are the ones related to N1m and N2v bursts duration, even though N1 do have some additional variability. This explains why the most variable one (similar to the period) is the N3N2 interval in this case, since it is the combination of N3 and N1 burst intervals.

Regarding the figure for the linear correlations with the period, consequent results to these variability effects

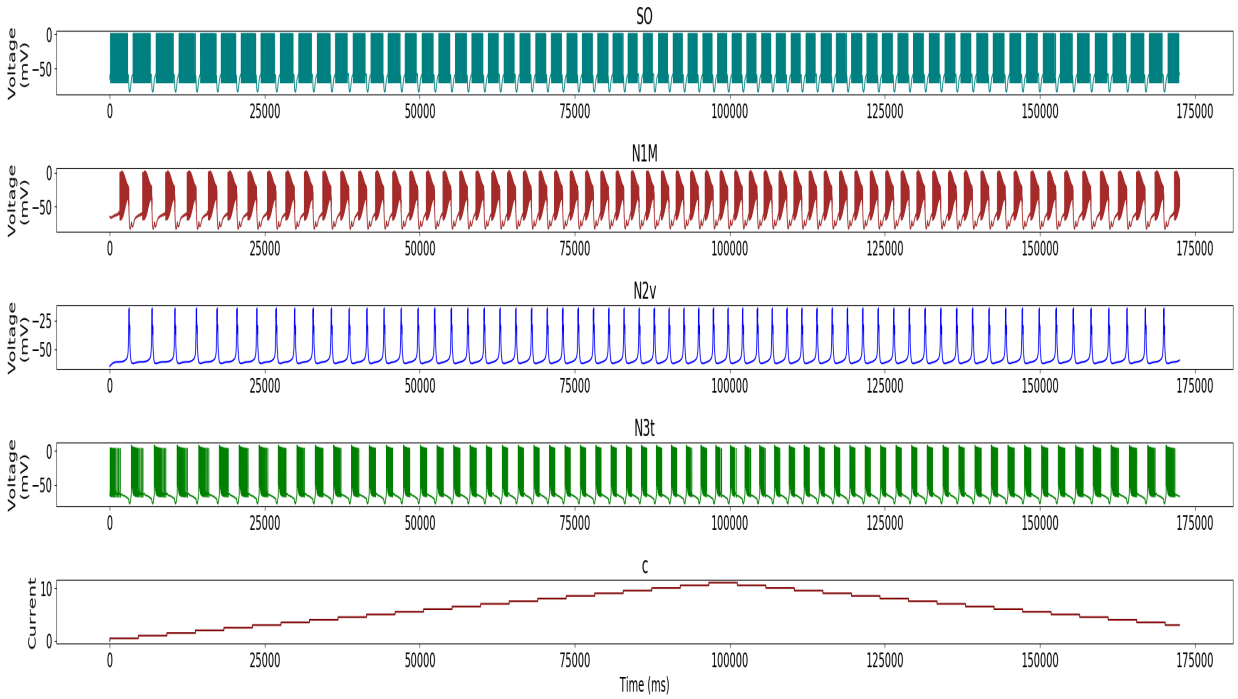

Figure 34: Complete circuit applying different I_{inj} values to N1M.

are observed. The first row displays burst duration intervals, which are the intervals analysed in Elliot et al. [Elliott and Andrew, 1991] from data obtained in *in vivo* recordings and in Vavoulis et al. from data obtained in model simulations [Vavoulis et al., 2007]. The results shown here match those results, being the third phase the most variable one. Due to this variability, is also highly correlated with the period, while the two other phases have small variation and, thus, are not related to period interval changes.

The most variable intervals identified, derived from other time references, show also a high correlation with the period in this figure. Therefore, since the ones involving N3 burst duration are the most correlated to the period, interval changes seem to be due to N3 variability.

On the other hand, intervals related to neuron N2 are the ones less variable. This neuron is the one less affected by the global activity of the circuit, in terms of its burst duration. Moreover, some of the intervals are too small, or even negative, since the end of one of the neuron activity overlaps the next one's beginning. This is the case for N1-N2 and N3-N1 delay (4th row, 1st column and 6th row, 2nd column, respectively).

As a complement to the other two figures in this section, the following table summarizes each phase stats, including R-squared value, and the mean and standard deviation for the three burst intervals, taking into account burst duration, interburst interval (IBI) and period.

Neuron	R^2		Duration	IBI	Period
N1	0.7467	**Mean**	1.1237	1.5354	2.6577
		Std	0.0576	0.5423	0.5896
N2	0.3578	**Mean**	0.2819	2.3775	2.6595
		Std	0.0008	0.5930	0.5935
N3	0.9760	**Mean**	1.1568	1.4959	2.6595
		Std	0.5277	0.1081	0.5935

Table 4: Statistics results from N1m-driven activity, in seconds.

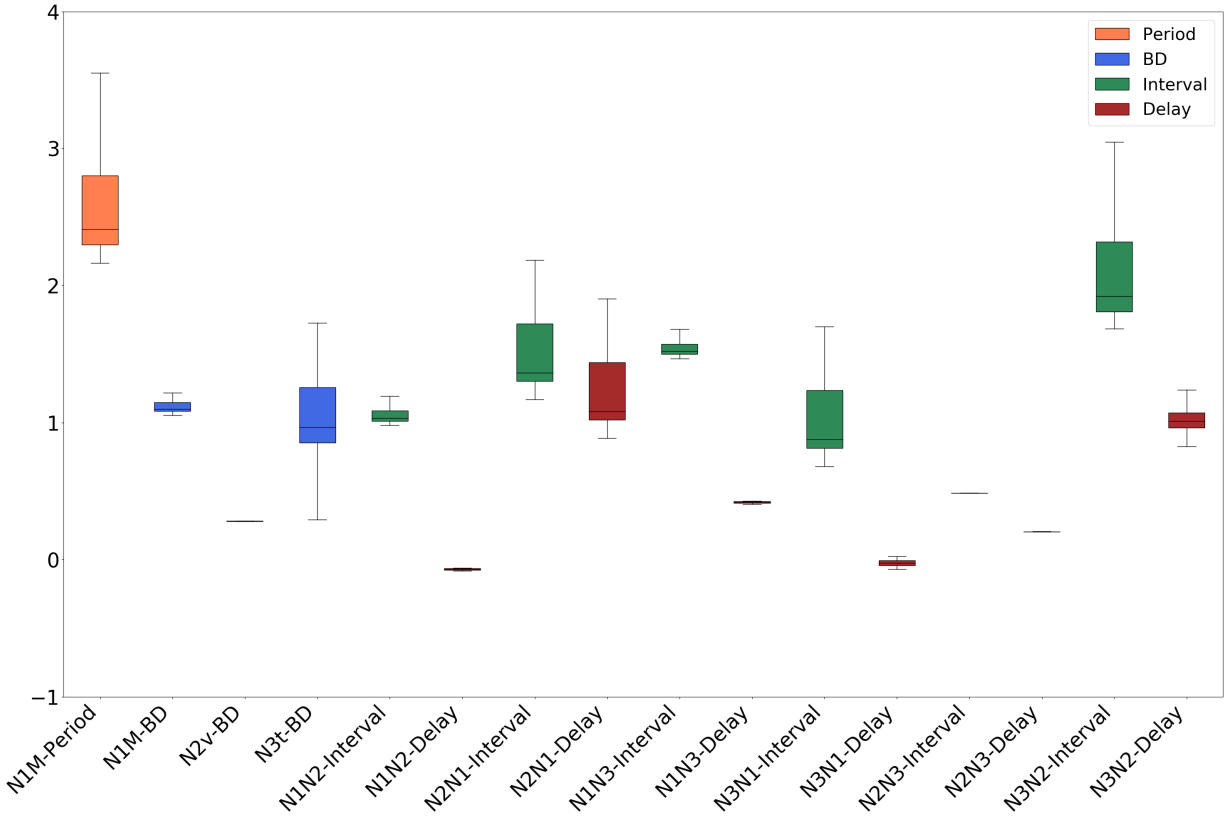

Figure 35: Box-plot intervals variation fro N1m simulation

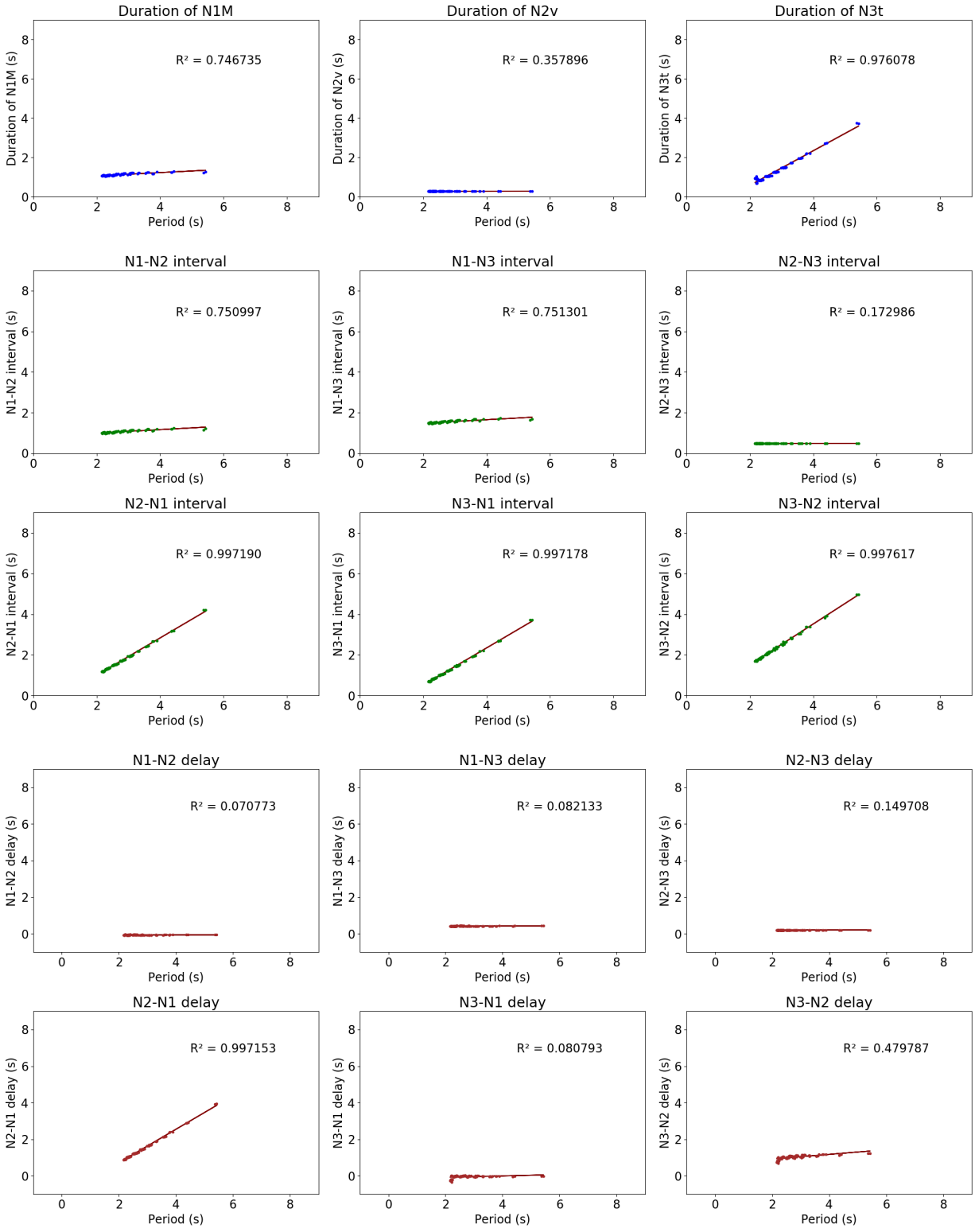

Figure 36: Intervals correlations to Period for N1m-driven simulation. First row: Burst duration. Second and third row: Two neurons intervals. Forth and Fifth: Two neurons delays.

3.2.2 SO driven activity

To simulate SO driven activity, the same protocol was implemented with a gradually increasing and decreasing current applied to SO to induce variability. Some parameter tuning was needed here. The minimum current value for SO to generate a burst was aprox. 8.2, so the injected current ranged from 8.2 to 13. and the current step change was also lower, set at 0.1. This current was applied to SO with the rest of the neurons with the same I_{inj} value as in the N1m driven activity (see 3.2.1). However this simulation did not obtain the same invariant results as in the previous case, neither the correlations shown in Vavoulis et al. [Vavoulis et al., 2007]. Figure 37 displays the whole circuit activity. As it can be appreciated here, N3t is barely variable, while N1m is the most variable one. This is corroborated in figure 38, where the correlation between the burst duration and the period for each of the neurons is exposed. N1m correlation is the highest, whereas N3t has a high value, but not as remarkable.

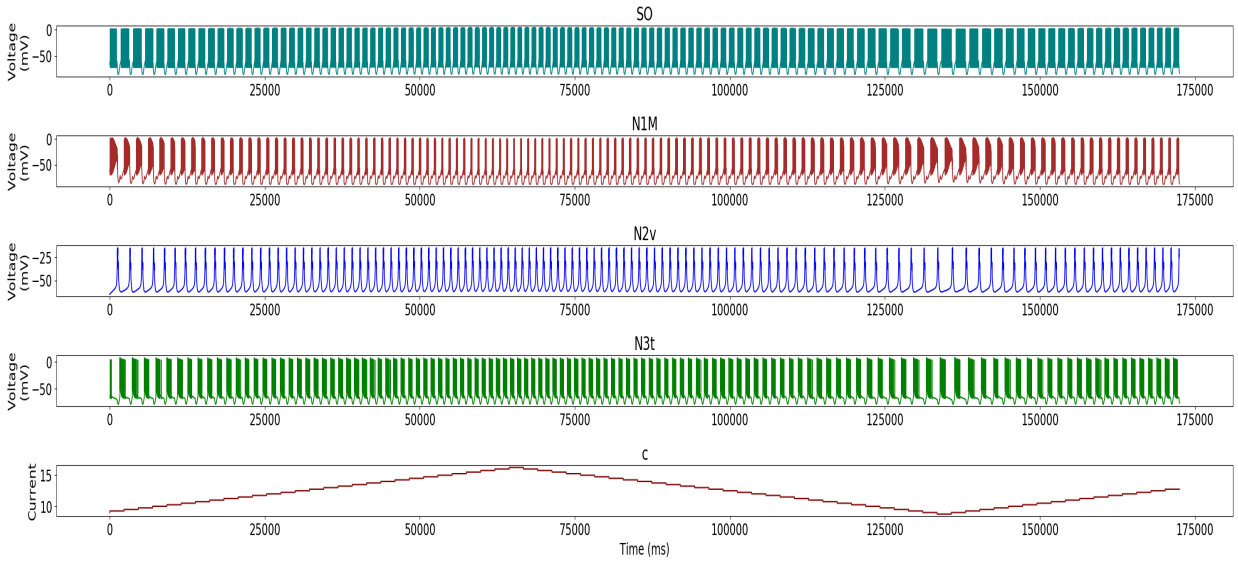

Figure 37: Complete circuit activy when applying different I_{inj} values to SO.

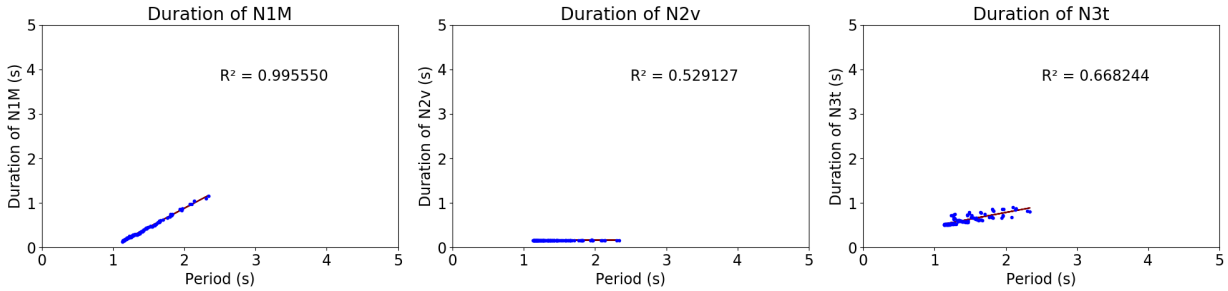

Figure 38: Burst duration correlations to Period for SO-driven simulation with $I_{inj} = 0$ for N3t.

In order to reproduce the results in [Vavoulis et al., 2007], where both N1M and N3t present variability, it is necessary to adjust parameters, so that N3t activity is strong enough to adapt to SO variability and carry

period information jointly to N1m. This way, N3t kept a constant I_{inj} value, since, regarding the effect of this parameter into this neuron (see 2.3.3), if a higher value is applied, the firing rate increases, so it will be harder for N1M to inhibit N3t. Thus, N3t value was changed from 0 to 4. On the other hand, the injected current in N2v controls burst frequency, increasing proportionally to the current. Therefore, N2v was also decreased from 2 to 1, so that SO burst could be longer.

To sum up, injected values for each neuron was finally set as follows: N1m=10; N2v=1; N3t=4; and SO injection dynamically changed with the c value. The result of this set up is displayed in figure 39. In this case, N3t variability was higher and the period was driven by both N1m and N3t.

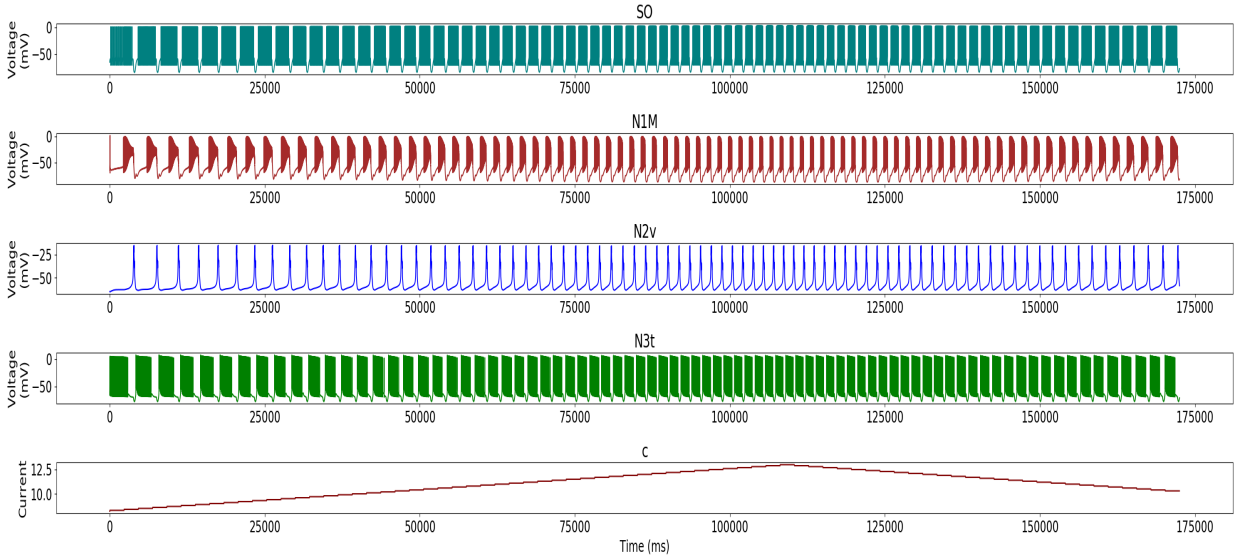

Figure 39: Complete circuit applying different I_{inj} values to SO. N3t $I_{inj} = 4$

With these simulation results, we have performed the same analyses as in the previous section. Events were detected and all intervals were measured and their variability was characterised in figures 15 and 14.

Figure 40 shows a box-plot representing interval variability, similar to the ones used for N1M-driven activity and the intracellular recordings. However, here we found more intervals showing high variability. N2 intervals, as it happened in the previous results, show low variability, which indicates that period variability is more likely a consequence of N3 and N1 activity. These two neurons show high variability in their burst duration intervals, being N1 even more variable than N3, while it was the other way round in previous results with distinct stimulation. All intervals derived from these two have high variability and a similar distribution in all of them. In spite all this, what remains constant from N1m-driven simulation is the variability of the N3-N2 interval, which includes both N1 and N3 burst duration, being N3-N2 the most variable one, and the closest to period variability.

Hence, as it happened in the previous results, the intervals with more variability and, thus, those that had a more similar distribution to period, were the ones that showed a highest linear relation to the period. Since in this case there are more neurons showing variability, we should expect finding more correlations when plotting each interval against the period.

Figure 41 displays the corresponding correlation analyses. Here we find the intervals correlation panel that

we have also discussed in the results reported in previous subsections. However, in this case we find different results, since period information, as we have just seen, seems to no longer be carried only by N3. Hence, we find correlations in the same intervals as before: N2-N1, N3-N1, N3-N2 intervals and N2-N1 delay; which are the intervals related to N3 burst duration. However, N1-N2, N1-N3 intervals and N3-N2 delay are also highly correlated to the period. These intervals are the ones related to N1 neuron activity.

Furthermore, it is important to notice that N3-N1 delay is negative, up to -1 in the scale. This means that there is a constant overlapping between N3 and N1 in each cycle.

Compared to N1m-driven results, there is another difference in period and burst duration, which is about half of the previous analysis. When driving the rhythm with SO, burst duration is much shorter, so the period and the rest of intervals are consequently smaller.

Hence, when driving the rhythm by SO, the model produces a rhythm where the period duration information seems to be carried by N3t as well as by N1M. This reproduces the experimentally analysed effect set out in [Elliott and Andrew, 1991].

The following table summarizes each phase stats, including R-squared value, and the mean and standard deviation for the three burst intervals, taking into account burst duration, interburst interval (IBI) and period.

Neuron	R^2		**Duration**	**IBI**	**Period**
N1	0.9627	**Mean**	0.8607	1.2498	2.1077
		Std	0.2947	0.18698	0.4679
N2	0.7030	**Mean**	0.1702	1.9305	2.1008
		Std	0.0029	0.4572	0.4548
N3	0.9374	**Mean**	1.4376	0.6650	2.1009
		Std	0.2529	0.2188	0.4549

Table 5: Statistics results from SO-driven activity, in seconds.

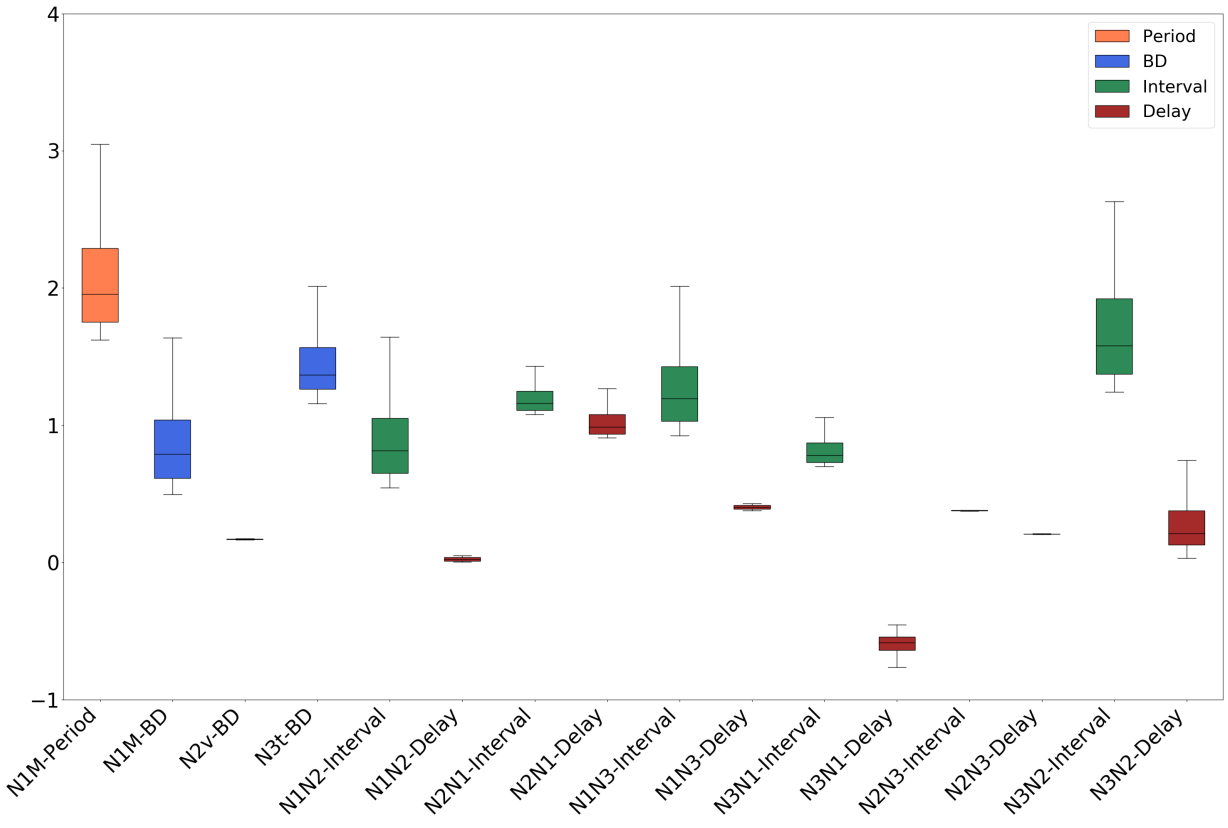

Figure 40: Box-plots of interval variability from SO-driven simulation.

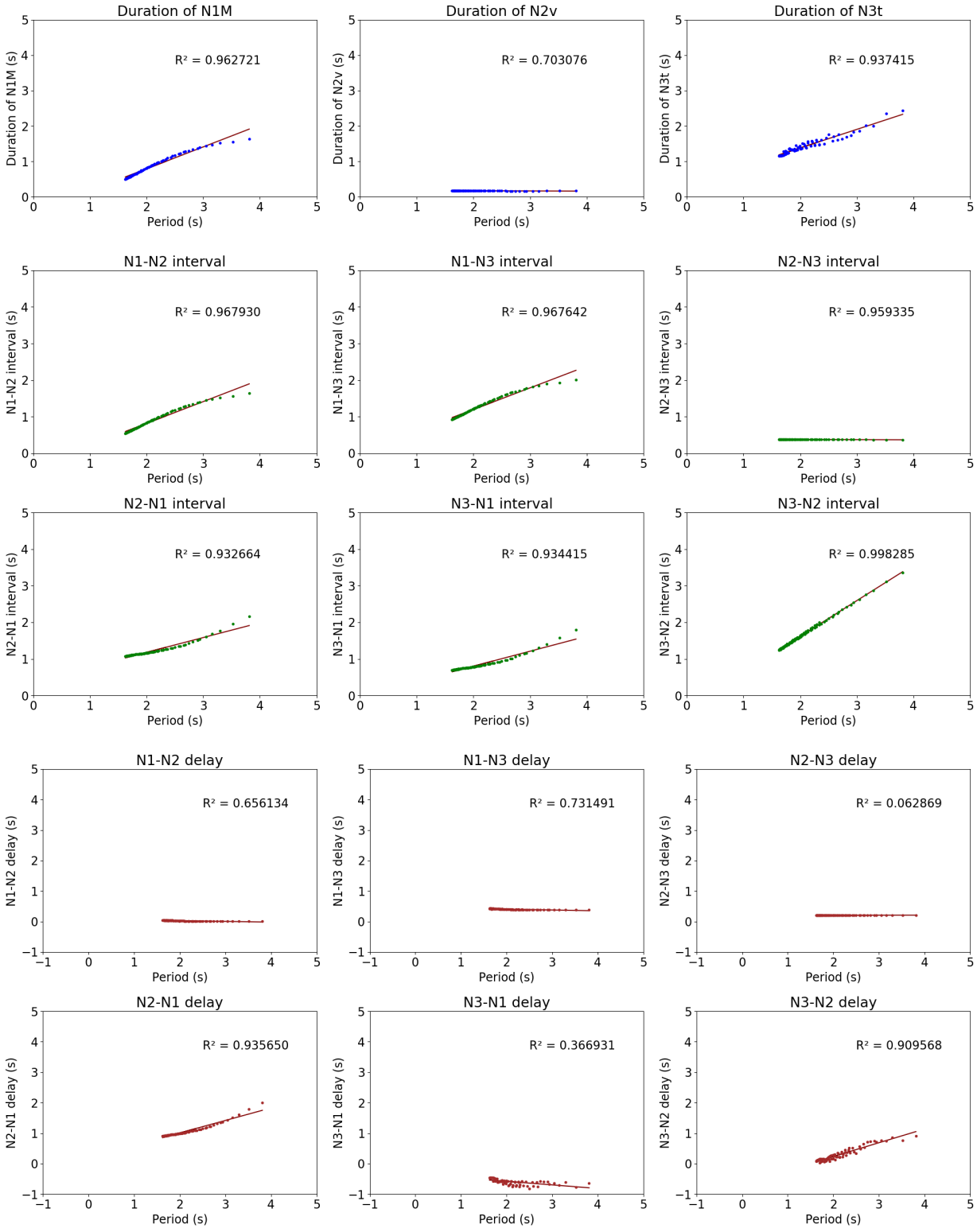

Figure 41: Intervals correlations to Period for SO-driven simulation. First row: Burst duration. Second and third row: Two-neuron intervals. Forth and Fifth row: Two-neurons delays.

4 Discussion

Along this document, we have addressed the characterisation of the intervals building up the sequence of the rhythms of the central pattern generator present in the feeding system in *Lymnaea Stagnalis*, both from *in vivo* recordings and from computational models describing its behaviour. This characterisation has also included the study of the presence of dynamical invariants in the form of linear relationships between the sequence intervals and the cycle period of the rhythm [Elices et al., 2019].

On the one hand, for the living neuron recordings, electrophisiological techniques were used, carrying out experiments involving intracellular and extracelullar recordigns on the isolated neural system. In the analysis of the intracellular recordings, we identified three different phases (N1,N2,N3) from two simultaneous recordings: one phase from the recording of one of the neurons (N1), and the other two phases from the recording of the second cell (N2,N3). Thanks to a significant change in firing rate frequency in each burst of the second recording, it was possible to differentiate between the two phases (N2,N3) of this second recording. Since these three phases were assumed to correspond to the each one of the three phases in the CPG, all intervals building the sequence were analysed in terms of variability and compared to the period in a cycle-by-cycle manner obtaining linear relations in several cases.

The results found in these recordings go along with the phenomena exposed in Elliot et al. [Elliott and Andrew, 1991] where in a recording from the spontaneous feeding rhythm in *Lymnaea* buccal ganglia, a high correlation between the period and the third phase was reported. In this work, we have extended this analysis by characterizing each interval building the sequence and relating the linear relations found to the concept of cycle-by-cycle dynamical invariants proposed in [Elices et al., 2019] for the coordination of robust yet flexible CPG rhythms.

On the other hand, for computational model simulations, two main cases have been addressed in the analysis: N1M-driven and SO-driven activity. This was based on the two different possibilities of inducing variability in the model according to the results reported in [Vavoulis et al., 2007]. When variability is driven by the stimulation of N1M, the results are rather similar to the ones obtained in intracelullar recordings, being N1M a bit more variable. Therefore, linear correlations are present, mainly in all intervals related to N3 burst duration, since those are the ones with a variability distribution more similar to the period.

When the stimulation is applied on SO, i.e., this neuron is inducing the variability, a different rhythm variability distribution is found, since there are more intervals presenting variability. This is due to the specific variability of N1M and N3t burst durations, since in this case period information seems to be carried not only by N3t but also N1M. Hence, consequently to the variability analyses, different linear relations are found, involving all intervals related to N3t and N1M. The intervals not showing relation with the period are the ones related to N2v, which is also the less variable entity.

These results reproduce and extend the ones discussed in [Vavoulis et al., 2007] and [Elliott and Andrew, 1991]. It is interesting to highlight the differences in the result when the period is driven by N1M or SO. When the variability is induced in N1M, N3t is still able to inhibit N1M carrying the main variability, while SO is adapting to both. However, when SO is the one stimulated, since it is connected to N1M by mutual excitation, they are both boosting each other's activity, leading to a higher variability of N1M. Here, N3t must adapt to N1M, what is harder due to the SO constant excitation. For this reason, it was necessary to inject some additional current in N3t, which would usually be an effect received from the cerebral ganglia.

As it was explained in section 1.3, each of the three phases here exposed correspond to a specific motor action: N1 protraction, N2 rasp and N3 swallow. As it is pointed out in [Elliott and Andrew, 1991], these phases are an example of two-stroke relaxation, which would be divided in protraction and rasp (N1,N2), in charge of moving the radula and swallowing (N3). In these kind of systems, it is usual to find one of them fixed and the other one variable, in our case it would be the swallow one. In this line, SO stimulation is related to sucrose stimulation [Benjamin, 2012, Rose and Benjamin, 1981], this could be related with the

increase in N1M variability, since in presence of food, protraction phase may get more important for a better food reaching. Thus, there might be now two phases showing more variability in their intervals duration. The discussed invariants can participate in the coordination of these mechanisms of motor coordination.

In this master thesis, the study of cycle-by-cycle invariant relationships, found not only in experimental recordings but also in computational models, highlights the presence of organised variability in a motor rhythm. Previous results that indicated the existence of these invariants in *Lymnaea Stagnalis* have been reproduced, providing a wider analysis of variability, not only in the burst duration intervals but in a complete set of intervals obtained from the relation between different neurons in dual recordings.

The presence of dynamical invariants in other CPGs beyond the already found in *Carcinus maenas* [Elices et al., 2019], points out to a general phenomena that can be present in other more complex neural systems. Moreover, the results indicate that invariants can be found in a computational model, which is not trivial because of the lack of sources for flexibility in theoretical paradigms. In this study, variability was induced by external stimulation into single neurons. It is important to emphasise that in the Vavoulis et al. model, variability is induced by applying a variable current to N1M or SO, being quite constant when this current is fixed.

As future work, it will be interesting to analyse key elements generating this invariant into the model and a comparison between this one and other models which cannot reproduce the invariants. Regarding the *in vivo* recordings, it will be necessary to move forward into the identification of neurons for a more precise characterisation of the rhythm and the antiphase sequential activations so the results shown here can be analysed under different behavioural conditions.

References

[dat,] DataView home: https://www.st-andrews.ac.uk/ wjh/dataview/index.html.

[pyt,] Python.org: https://www.python.org/.

[Amaducci et al., 2019] Amaducci, R., Reyes-Sanchez, M., Elices, I., Rodriguez, F. B., and Varona, P. (2019). RThybrid: A standardized and open-source real-time software model library for experimental neuroscience. *Frontiers in Neuroinformatics*, 13:1–14.

[Arichi et al., 2017] Arichi, T., Whitehead, K., Barone, G., Pressler, R., Padormo, F., Edwards, A. D., and Fabrizi, L. (2017). Localization of spontaneous bursting neuronal activity in the preterm human brain with simultaneous EEG-fMRI. *eLife*, 6:1–14.

[Arroyo et al., 2013] Arroyo, D., Chamorro, P., Amigó, J. M., Rodríguez, F. B., and Varona, P. (2013). Event detection, multimodality and non-stationarity: Ordinal patterns, a tool to rule them all? *The European Physical Journal Special Topics*, 222(2):457–472.

[Bauer et al., 2014] Bauer, J. A., Lambert, K. M., and White, J. A. (2014). The past, present, and future of real-time control in cellular electrophysiology. *IEEE Transactions on Biomedical Engineering*, 61(5):1448–56.

[Benjamin et al., 1979] Benjamin, B. Y. P. R., Rose, R. M., Slade, C. T., Lacy, M. G., BENJAMIN, P. R., Rose, R. M., Slade, C. T., and Lacy, M. G. (1979). Morphology of Identified Neurones in the Buccal Ganglia of Lymnaea Stagnalis. *Journal of Experimental Biology*, 80(1):119–135.

[Benjamin, 2012] Benjamin, P. R. (2012). Distributed network organization underlying feeding behavior in the mollusk Lymnaea. *Neural Systems & Circuits*, 2(1):1–16.

[Brette and Destexhe,] Brette, R. and Destexhe, A. Intracellular recording. In Brette, R. and Destexhe, A., editors, *Handbook of Neural Activity Measurement*, chapter 3, pages 44–91. Cambridge University Press, Cambridge.

[Chamorro et al., 2012] Chamorro, P., Muñiz, C., Levi, R., Arroyo, D., Rodríguez, F. B., and Varona, P. (2012). Generalization of the dynamic clamp concept in neurophysiology and behavior. *PLoS ONE*, 7(7):e40887.

[Cole, 1955] Cole, K. S. (1955). Ions, potentials and the nerve impulse. In Shedlovsky, T., editor, *Electrochemistry in biology and medicine*, chapter Ions, pote, pages 121–140. Wiley, New York.

[Dehaene, 2014] Dehaene, S. (2014). *Consciousness and the brain : deciphering how the brain codes our thoughts*. Penguin.

[Destexhe et al., 1994] Destexhe, A., Mainen, Z. F., and Sejnowski, T. J. (1994). An Efficient Method for Computing Synaptic Conductances Based on Kinetic Model of Receptor Binding. *Neural Computation*, 6:14–18.

[Dimitrijevic et al., 1998] Dimitrijevic, M. R., Gerasimenko, Y., and Pinter, M. M. (1998). Evidence for a spinal central pattern generator in humans. *Annals of the New York Academy of Sciences*, 860:360–76.

[Elices et al., 2019] Elices, I., Levi, R., Arroyo, D., Rodriguez, F. B., and Varona, P. (2019). Robust dynamical invariants in sequential neural activity. *Scientific Reports*, 9(1).

[Elices and Varona, 2015] Elices, I. and Varona, P. (2015). Closed-loop control of a minimal central pattern generator network. *Neurocomputing*, 170:55–62.

[Elices and Varona, 2017] Elices, I. and Varona, P. (2017). Asymmetry Factors Shaping Regular and Irregular Bursting Rhythms in Central Pattern Generators. *Frontiers in Computational Neuroscience*, 11:9.

[Elliott and Andrew, 1991] Elliott, B. Y. C. J. H. and Andrew, T. (1991). Temporal Analysis of Snail Feeding Rhythms: a Three-Phase Relaxation Oscillator. *Journal of Experimental Biology*, 157(1):391–408.

[Fairhall and Machens, 2017] Fairhall, A. and Machens, C. (2017). Editorial overview: Computational neuroscience. *Current Opinion in Neurobiology*, 46:A1–A5.

[Fernandez-Vargas et al., 2013] Fernandez-Vargas, J., Pfaff, H. U., Rodriguez, F. B., and Varona, P. (2013). Assisted closed-loop optimization of SSVEP-BCI efficiency. *Frontiers in Neural Circuits*, 7:Article 27.

[Galvani, 1791] Galvani, L. (1791). *De viribus electricitatis in motu musculari: Commentarius. Bologna: Press of the Academy of Sciences.*

[Garrido Peña, 2019] Garrido Peña, A. (2019). TFM Part 2: Design and implementation of hybrid circuits in Lymnaea stagnalis.

[Grech et al., 2008] Grech, R., Cassar, T., Muscat, J., Camilleri, K. P., Fabri, S. G., Zervakis, M., Xanthopoulos, P., Sakkalis, V., and Vanrumste, B. (2008). Review on solving the inverse problem in EEG source analysis. *Journal of Neuroengineering and Rehabilitation*, 5:25.

[Grosenick et al., 2015] Grosenick, L., Marshel, J., and Deisseroth, K. (2015). Closed-Loop and Activity-Guided Optogenetic Control. *Neuron*, 86(1):106–139.

[Hartline and Maynard, 1976] Hartline, D. K. and Maynard, D. M. (1976). Mottor patterns in the stomatogastric ganglion of the lobster Panulirus argus. *J. Exp. Biol.*, 62(2):405–420.

[Heitler, 2007] Heitler, W. J. (2007). DataView: A Tutorial Tool for Data Analysis. Template-based Spike Sorting and Frequency Analysis. *Journal of Undergraduate Neuroscience Education*, 6(1):1–7.

[Herrero-Carrón et al., 2011] Herrero-Carrón, F., Rodríguez, F., and Varona, P. (2011). Bio-inspired design strategies for central pattern generator control in modular robotics. *Bioinspiration and Biomimetics*, 6(1):16006.

[Hodgkin and Huxley, 1952] Hodgkin, A. L. and Huxley, A. F. (1952). A quantitative description of membrane current and its application to conduction and excitation in nerve. *The Journal of physiology*, 117(4):500–44.

[Huerta et al., 2001] Huerta, R., Varona, P., Rabinovich, M., and Abarbanel, H. (2001). Topology selection by chaotic neurons of a pyloric central pattern generator. *Biological Cybernetics*, 84(1):L1—-L8.

[Kandel et al., 2012] Kandel, E. R., Schwartz, J. H., and Jessell, T. M. (2012). *Principles of Neural Science*. McGraw-Hill Education, New York, 5 edition.

[Karahanoğlu and Van De Ville, 2017] Karahanoğlu, F. I. and Van De Ville, D. (2017). Dynamics of Large-Scale fMRI Networks: Deconstruct Brain Activity to Build Better Models of Brain Function. *Current Opinion in Biomedical Engineering*, 3:28–36.

[Katz and Quinlan, 2019] Katz, P. S. and Quinlan, P. D. (2019). The importance of identified neurons in gastropod molluscs to neuroscience. *Current Opinion in Neurobiology*, 56:1–7.

[Kiebel et al., 2009] Kiebel, S. J., von Kriegstein, K., Daunizeau, J., and Friston, K. J. (2009). Recognizing sequences of sequences. *PLoS computational biology*, 5(8):e1000464.

[Komendantov and Kononenko, 1996] Komendantov, A. O. and Kononenko, N. I. (1996). Deterministic chaos in mathematical model of pacemaker activity in bursting neurons of snail, Helix pomatia. *Journal of Theoretical Biology*, 183(2):219–230.

[Lago-Fernández et al., 2009] Lago-Fernández, L., Szücs, A., and Varona, P. (2009). Determining burst firing time distributions from multiple spike trains. *Neural Computation*, 21(4).

[Latorre et al., 2013] Latorre, R., Aguirre, C., Rabinovich, M., and Varona, P. (2013). Transient dynamics and rhythm coordination of inferior olive spatio-temporal patterns. *Frontiers in Neural Circuits*, 7(SEP):138.

[Latorre et al., 2006] Latorre, R., Rodríguez, F. B., and Varona, P. (2006). Neural signatures: multiple coding in spiking-bursting cells. *Biol Cybern*, 95(2):169–183.

[Patel et al., 2017] Patel, Y. A., George, A., Dorval, A. D., White, J. A., Christini, D. J., and Butera, R. J. (2017). Hard real-time closed-loop electrophysiology with the Real-Time eXperiment Interface (RTXI). *PLOS Computational Biology*, 13(5):e1005430.

[Pavlidis et al., 2016] Pavlidis, E., Cantalupo, G., Cattani, L., Tassinari, C. A., and Pisani, F. (2016). Neonatal seizure automatism and human inborn pattern of quadrupedal locomotion. *Gait and Posture*, 49:232–234.

[Potter et al., 2014] Potter, S. M., El Hady, A., and Fetz, E. E. (2014). Closed-Loop Neuroscience and Neuroengineering. *Frontiers in Neural Circuits*, 8(115).

[Rabinovich et al., 2010] Rabinovich, M. I., Afraimovich, V. S., and Varona, P. (2010). Heteroclinic Binding. *Dynamical Systems: An International Journal*, 25(3):433–442.

[Rabinovich et al., 2006] Rabinovich, M. I., Varona, P., Selverston, A. I., and Abarbanel, H. D. I. (2006). Dynamical principles in neuroscience. *Reviews of Modern Physics*, 78(4):1213–1265.

[Reyes-Sanchez et al., 2018] Reyes-Sanchez, M., Amaducci, R., Elices, I., Rodriguez, F. B., and Varona, P. (2018). Automatic adaptation of model neurons and connections to build hybrid circuits with living networks. *bioRxiv*, page 419622.

[Robinson and Kawai, 1993] Robinson, H. P. and Kawai, N. (1993). Injection of digitally synthesized synaptic conductance transients to measure the integrative properties of neurons. *Journal of Neuroscience Methods*, 49:157.

[Rose and Benjamin, 1981] Rose, R. and Benjamin, P. (1981). Interneuronal control of feeding in the pond snail lymnaea stagnalis: I. initiation of feeding cycles by a single buccal interneurone. *J. Exp. Biol.*, 92.

[Selverston et al., 2000] Selverston, A. I., Rabinovich, M. I., Abarbanel, H. D. I., Elson, R., Szücs, A., Pinto, R. D., Huerta, R., and Varona, P. (2000). Reliable circuits from irregular neurons: a dynamical approach to understanding central pattern generators. *Journal of Physiology-Paris*, 94(5-6):357–374.

[Sharp et al., 1993] Sharp, A. A., O'Neil, M. B., F, A. L., and E, M. (1993). The dynamic damp: artificial condudances in biological neurons. *Tins*, 16:389–394.

[Staras et al., 1998] Staras, K., Kemenes, G., and Benjamin, P. R. (1998). Pattern-generating role for motoneurons in a rhythmically active neuronal network. *Journal of Neuroscience*, 18(10):3669–3688.

[Straub et al., 2002] Straub, V. A., Staras, K., Kemenes, G., and Benjamin, P. R. (2002). Endogenous and network properties of Lymnaea feeding central pattern generator interneurons. *Journal of Neurophysiology*, 88(4):1569–1583.

[Szücs et al., 2000] Szücs, A., Varona, P., Volkovskii, A., Abarbanel, H., Rabinovich, M., and Selverston, A. (2000). Interacting Biological and Electronic Neurons Generate Realistic Oscillatory Rhythms. *Neuroreport*, 11(3):563–569.

[Torres and Varona, 2012] Torres, J. J. and Varona, P. (2012). Modeling Biological Neural Networks. In *Handbook of Natural Computing*, volume 1-4, pages 533–564. Springer, Berlin, Heidelberg.

[Varona et al., 2016] Varona, P., Arroyo, D., Rodríguez, F. B., and Nowotny, T. (2016). Online event detection requirements in closed-loop neuroscience. In El Hady, A., editor, *Closed-Loop Neuroscience*, pages 81–91. Academic Press.

[Varona and Rabinovich, 2016] Varona, P. and Rabinovich, M. I. (2016). Hierarchical dynamics of informational patterns and decision-making. *Proceedings of the Royal Society B*, 283(1832):20160475.

[Varona et al., 2001a] Varona, P., Torres, J., Huerta, R., Abarbanel, H., and Rabinovich, M. (2001a). Regularization mechanisms of spiking-bursting neurons. *Neural Networks*, 14(6-7):865–875.

[Varona et al., 2001b] Varona, P., Torres, J. J., Abarbanel, H., Rabinovich, M., and Elson, R. (2001b). Dynamics of two electrically coupled chaotic neurons: experimental observations and model analysis. *Biological Cybernetics*, 84(2):91–101.

[Vavoulis et al., 2007] Vavoulis, D. V., Straub, V. A., Kemenes, I., Kemenes, G., Feng, J., and Benjamin, P. R. (2007). Dynamic control of a central pattern generator circuit: A computational model of the snail feeding network. *European Journal of Neuroscience*, 25(9):2805–2818.

[Vehovszky et al., 2004] Vehovszky, , Szabó, H., and Elliott, C. J. (2004). Octopamine-containing (OC) interneurons enhance central pattern generator activity in sucrose-induced feeding in the snail Lymnaea. *Journal of Comparative Physiology A: Neuroethology, Sensory, Neural, and Behavioral Physiology*, 190(10):837–846.

[Venaille et al., 2005] Venaille, A., Varona, P., and Rabinovich, M. I. (2005). Synchronization and coordination of sequences in two neural ensembles. *Physical Review E*, 71(6 Pt 1):61909.